The structural basis of modified nucleosome recognition by 53BP1

The structural basis of modified nucleosome recognition by 53BP1

Marcus D. Wilson[1]*, Samir Benlekbir[2]*, Amélie Fradet-Turcotte[1,3], Alana Sherker[1,4], Jean-Philippe Julien[2,5,6], Andrea McEwan[1], Sylvie M. Noordermeer[1], Frank Sicheri[1,4,5#], John L. Rubinstein[2,5,7#], and Daniel Durocher[1,4#]

[1]The Lunenfeld-Tanenbaum Research Institute, Mount Sinai Hospital, 600 University Avenue, Toronto, ON, M5G1X5 Canada.
[2]Molecular Structure and Function Program, The Hospital for Sick Children Research Institute, Toronto, ON M5G 0A4, Canada.
[3]Present address: Laval University Cancer Research Center, Oncology Axis-CHU de Québec Research Center, Hôtel-Dieu de Québec, Quebec City, QC, G1R 2J6 Canada; Centre Hospitalier Universitaire de Québec Research Center – Université Laval, Quebec City, QC, Canada.
[4]Department of Molecular Genetics, University of Toronto, ON, M5S 3E1, Canada.
[5]Department of Biochemistry, University of Toronto, Toronto, Ontario, M5S 1A8, Canada.
[6]Department of Immunology, University of Toronto, Toronto, Ontario, M5S 1A8, Canada.
[7]Department of Medical Biophysics, University of Toronto, Toronto, Ontario, M5G 1L7, Canada.

* These authors contributed equally to this work

#Address correspondence to:

Frank Sicheri, Ph.D.
e-mail: sicheri@lunenfeld.ca

John Rubinstein, Ph.D.
e-mail: john.rubinstein@utoronto.ca

Daniel Durocher, Ph.D.
e-mail: durocher@lunenfeld.ca

DNA double-strand breaks (DSBs) elicit a histone modification cascade that controls DNA repair[1-3]. This pathway involves the sequential ubiquitylation of histones H1 and H2A by the E3 ubiquitin ligases RNF8 and RNF168, respectively[4-8]. RNF168 ubiquitylates H2A on Lys-13 and Lys-15[7,8] (yielding H2AK13ub and H2AK15ub), an event that triggers the recruitment of 53BP1 to chromatin flanking DSBs[9,10]. 53BP1 binds specifically to H2AK15ub-containing nucleosomes through a peptide segment termed the UDR, which requires the simultaneous engagement of histone H4 Lys-20 dimethylation (H4K20me2) by its tandem Tudor domain[10,11]. How 53BP1 interacts with these two histone marks in the nucleosomal context, how it recognizes ubiquitin, and how it discriminates between H2AK13ub and H2AK15ub is unknown. Here we present the electron cryomicroscopy structure of a 53BP1 dimer bound to a H4K20me2- and H2AK15ub-containing nucleosome core particle at 4.5 Å resolution. The structure reveals that H4K20me2 and H2AK15ub recognition involves intimate contacts with multiple nucleosomal elements including the acidic patch. Ubiquitin recognition by 53BP1 is unusual and involves the sandwiching of the UDR segment between ubiquitin and the NCP surface. The selectivity for H2AK15ub is imparted by two arginine fingers in the H2A N-terminal tail, which straddle the nucleosomal DNA and serve to position ubiquitin over the NCP-bound UDR segment. The NCP-ubme/GST-53BP1 complex structure reveals the basis of 53BP1 recruitment to DSB sites and illuminates how combinations of histone marks and nucleosomal elements cooperate to produce highly specific chromatin responses such as those elicited following chromosome breaks.

To elucidate the molecular basis of 53BP1 recruitment to the chromatin surrounding DNA breaks, we sought to determine the three-dimensional structure of a complex consisting of 53BP1 bound to an NCP modified with H4K20me2 and H2AK15ub (referred to as NCP-ubme). We incorporated a dimethyl-lysine

mimic by cysteine alkylation of a histone H4K20C mutant[12], yielding H4K$_C$20me2 (Extended Data Fig. 1a-b). In parallel, we produced H2AK15ub by enzymatic ubiquitylation of H2A K13R/K36R in the context of a H2A-H2B dimer[13] (Extended Data Fig. 1c-g). The K36R mutation prevented off-target ubiquitylation at this residue (Extended Data Fig. 1c; H2A-K13R/K36R is hereafter referred to as H2A). Re-purified H4K$_C$20me2 and H2AK15ub were reconstituted into histone octamers and then wrapped with a 145 bp fragment of '601' DNA[14] to form NCP-ubme (Extended Data Fig. 1h).

The minimal 53BP1 fragment recruited to DSB sites consists of a dimer of the tandem Tudor-UDR segment[10] (residues 1484-1631, Extended Data Fig. 2a). We employed GST as a dimerization module to produce a Tudor-UDR dimer (hereafter termed GST-53BP1, Extended Data Fig. 2a). GST-53BP1 bound to NCP-ubme with a K_D of 1 μM, with only a ~2-fold reduction in association compared to a 53BP1 fragment containing the native oligomerization domain (Extended Data Fig. 2c-e). The resulting GST-53BP1 protein formed a stable complex with NCP-ubme with a 2: 1 (53BP1:NCP-ubme) stoichiometry (Fig. 1a and Extended Data Fig. 2eg).

We determined the structure of the NCP-ubme/GST-53BP1 complex by single particle electron cryomicroscopy (cryo-EM) at 4.5 Å resolution (Fig. 1bc and Extended Data Fig. 3). The rigid nucleosome forms a symmetrical coin shape consistent with other NCP-protein structures[3,15-19], with extra density attributable to ubiquitin and 53BP1 on each face of the NCP. The densities from the DNA and core secondary structural elements of the histones were

unmistakable and similar to previous NCP models[14,20] (RMSD 0.95 Å). The NCP density was sufficiently detailed to model several bulky side-chains (Extended Data Fig. 3g) and the path of the H2A N-terminal tail (see below). Ubiquitin was fit unambiguously into the cryo-EM map, linked via an isopeptide bond to H2A Lys-15. No extra density was visualized for the GST moiety, which is likely located near the nucleosome dyad (Extended Data Fig. 3h). The cryo-EM density for the tandem Tudor domain of 53BP1 was weaker than the rest of the structure but its center of mass was fixed over the tail of H4, consistent with its tethering to H4K$_C$20me2 (Fig. 1b).

We attributed extra density projecting from the tandem Tudor domain to residues 1610-1631 of the 53BP1 UDR. This region traverses ~50 Å across the NCP, forming contacts with both ubiquitin and histone surfaces (Fig. 1b-d). From its N terminus, the UDR snakes along the NCP-ubme surface, first across a solvent-exposed cleft formed between H4 and H2B, and then through a channel formed between the hydrophobic patch of ubiquitin and the NCP exterior. The UDR continues over the H2B αC helix, over His-108 and Lys-109, and terminates in a predicted helical conformation above the H2A-H2B acidic patch. While we were unable to unambiguously assign the UDR density, we deduced the sequence register of the UDR based on complementarity to the local physicochemical environment and by mutational studies described below (Fig. 1d).

We also determined the structure of the unliganded NCP-ubme at 7.7 Å resolution (Extended Data Fig. 4 and Fig. 2a). Comparison of ubiquitin in the

bound and unbound states (Fig. 2bc) suggests that ubiquitin becomes rigidly constrained upon 53BP1 binding following interaction with two separate interfaces: one containing the H2B αC helix and the other involving the UDR of 53BP1 (Fig. 2cd).

To facilitate validation of the NCP-ubme/GST-53BP1 structure, we substituted enzymatic ubiquitylation with chemical ubiquitylation of H2A[21] using a K15C mutant (Extended Data Fig. 5a-c). We first assessed the relevance of the ubiquitin interaction with the H2B αC helix, which encompasses H2B residues Lys-116, Thr-119 and Ser-123 (Fig. 2d, left and Extended Data Fig. 5d). As predicted, mutation of H2B Thr-119 to alanine (H2B T119A) or glutamate (H2B T119E), a phosphomimetic residue, greatly reduced binding of GST-53BP1 to NCP-ubme (Extended Data Fig. 5e-g). As H2B Thr-119 phosphorylation is detected during meiosis[22], our results suggest that this histone mark could inhibit 53BP1 recruitment to DSBs. Lys-120 of H2B lies in close proximity to the GST-53BP1-bound ubiquitin (Fig. 2d, left). This residue is ubiquitylated during transcriptional elongation and DSB induction[23-25], and may antagonize 53BP1 recruitment to chromatin[25]. We tested whether 53BP1 binding tolerates H2BK120 ubiquitylation and observed that NCPs containing H2BK120ub/H2AK15ub are efficiently bound by GST-53BP1 (Extended Data Fig. 5h). Therefore, it is unlikely that H2BK120 ubiquitylation directly blocks 53BP1 recruitment to chromatin.

RNF168 targets both H2A Lys-13 and Lys-15 in response to DSBs[7,8], but only H2AK15ub is recognized by 53BP1[10]. The NCP-ubme/GST-53BP1 structure hints at the basis for this specificity, which likely involves an interaction between

DNA and the N-terminal tail of H2A (Fig. 2d, right). The H2A residues Arg-11 and Arg-17 straddle the DNA at superhelical location 4.5, placing the Lys-15-tethered ubiquitin in a position to interact with the UDR. A similarly ordered H2A tail has been observed previously[26], suggesting it can adopt this conformation independently of ubiquitylation. Consistent with the H2A-tail conformation underpinning 53BP1 binding specificity, shifting the ubiquitylation site by 7 Å to H2AK13 reduced binding to GST-53BP1 (Extended Data Fig. 6a-c) and this binding was restored by a compensatory shift of the two arginine "fingers" in the H2A N-terminal tail sequence (Extended Data Fig. 6c and ref[10]).

The 28-residue UDR, C-terminal to the tandem Tudor domain, confers both ubiquitin and NCP recognition to 53BP1. Cross-linking experiments indicated that the C terminus of the UDR lies near the nucleosome acidic patch, while the N-terminal residues lie near to the H2B-H4 cleft (Extended Data Fig. 7ab). The Sir3 BAH domain also interacts with the H2B-H4 cleft[16], suggesting that this surface may be commonly exploited by NCP-binding proteins (Extended Data Fig. 7c).

In addition to H2B-ubiquitin interactions (Fig. 2d, left), direct interactions between the 53BP1 UDR and ubiquitin promote the constrained ubiquitin conformation. However, as the UDR shows no measurable affinity for free ubiquitin[10], these interactions are dependent on UDR binding to the NCP. Ubiquitin presents its hydrophobic patch (comprising Leu-8, Ile-44 and Val-70) towards the middle of the modeled UDR, centered on the aliphatic side chains of Ile-1617 and Leu-1619 of 53BP1 (Fig. 3a, left), which are also key residues for

53BP1 recruitment to DSB sites[10] (Fig. 3b and Extended Data Fig. 8ab). The I44A mutation in ubiquitin also reduced binding of GST-53BP1 to NCP-ubme, as observed previously[10] (Extended data Fig. 8c-e). The Lys-6 and His-68 side-chains of ubiquitin lie in proximity to two UDR residues, Asp-1616 and Asp-1620. Mutation of both acidic residues to lysine (D1616/1620K) reduced 53BP1 binding to NCP-ubme and impaired recruitment of 53BP1 to DSB sites (Fig. 3bc), while the K6E/H68E ubiquitin mutations impaired 53BP1 binding to NCP-ubme (Extended data Fig. 8c-e). Collectively, these results confirm that the unusual mode of ubiquitin recognition by 53BP1 involves the sandwiching of the UDR segment by the NCP surface and the ubiquitin moiety. They also suggest that K6-linked ubiquitin chains, if they occur on H2AK15, are incompatible with 53BP1 binding. However, as most other lysine residues of ubiquitin project away from the NCP-ubme/GST-53BP1 complex (Extended Data Fig. 8f), the 53BP1/NCP-ubme interaction may be permissive to H2AK15 poly-ubiquitylation.

The acidic patch acts as a nexus for protein binding to the nucleosome [13,15,16,18,19,27,28]. 53BP1 also takes advantage of this surface (Fig. 3a, right and Extended Data Fig. 9a) and its association to NCP-ubme can be outcompeted by the acidic patch-binding LANA peptide[19,27] (Extended Data Fig. 9b). Removal of the negative charge in the acidic patch, through H2A E61/91/92A and H2B E105A mutations, reduced GST-53BP1 binding to NCP-ubme (Fig. 3d and Extended Data Fig. 9cd). The C-terminal portion of the UDR is highly basic (Fig. 1d) and, in the modeled UDR, residues within the C-terminal α-helix are positioned to interact directly with the acidic patch (Fig. 3a, right). Mutation of any

of these residues (K1626A, R1627A, K1628C and K1629A) reduced binding of GST-53BP1 to NCP-ubme (Fig. 3e and Extended Data Fig. 9ef). In particular, the 53BP1 R1627A mutation, which also disables recruitment to DSB sites[10], had the most pronounced effect on binding, suggesting that this residue acts as the 'arginine-anchor'[15] (Extended Data Fig. 9fg). Mutation of UDR contact elements immediately adjacent to the acidic patch, Lys-108 and His-109 of H2B (Extended Data Fig. 9a) also decreased the affinity of GST-53BP1 for NCP-ubme (Fig. 3d), emphasizing the role of this interaction surface for 53BP1 binding to chromatin.

The cryo-EM density above the methylated H4 tail was weaker than that of the rest of the NCP-ubme/GST-53BP1 structure (Fig. 4ab) and did not readily fit the crystal structure of the 53BP1 tandem Tudor domain[11]. Different structures for this region were obtained from distinct 3D classes during image processing, with density in the shape of 'stem and blossom' features that we attribute to the site of engagement of H4K_C20me2 (Extended Data Fig. 10a). In all 3D classes, the H4 tail projects upwards, away from the NCP surface, where it engages the methyl-lysine binding pocket of the tandem Tudor domain (Fig. 4a). Since the GST-53BP1 I1617A protein, which is unable to bind to H2AK15ub (Fig. 3b), binds to both a short dimethylated H4 peptide and to NCP-ubme with comparable affinity (Fig. 4c and Extended Data Fig. 10bc), we surmise that the tandem Tudor domain interacts primarily with a short patch of the H4 tail independently of other nucleosomal elements.

Finally, we tested binding of a 53BP1 fragment that harbored its native oligomerization domain, instead of GST, to NCP-ubme variants. Each of the

elements of NCP-ubme necessary for GST-53BP1 binding is similarly necessary for binding to the native 53BP1 oligomers (Extended Data Fig. 10d). These results ascertained that the binding mode described for the GST-53BP1/NCP-ubme structure faithfully represents the binding of 53BP1 to nucleosomes.

In summary, the structure of 53BP1 bound to a methylated and ubiquitylated nucleosome highlights how a highly specific biological response, such as the recruitment of 53BP1 to DSB sites, is built from the multivalent engagement of histone post-translational modifications. Far from being the consequence of independent binding events to modified histone residues, the binding of 53BP1 to NCPs requires the coordinated involvement of multiple nucleosomal elements. We also speculate that the intimate association of the 53BP1 dimer with the nucleosome, coupled to its pincer-like binding mode that involves both faces of the nucleosome, may play a key role in stabilizing the nucleosomal barrier that inhibits DNA end resection[29].

Acknowledgements

We are grateful to R. Szilard for reading the manuscript. We thank M. Forbes for 1D mass spectrometry analysis, C. Davey for providing the 601 DNA, S. Orlicky and D. Ceccarelli for proteins, R. Guenette and E. Strieter for advice on H2A ubiquitylation and T. Sixma for discussions. MDW was supported by a Human Frontiers Science Program fellowship. SMN holds a fellowship of the Dutch Cancer Foundation (KWF). JLR is the Canada Research Chair (Tier 1) in Electron Cryomicroscopy and DD is a Canada Research Chair (Tier 1) in the

Molecular Mechanisms of Genome Integrity. Work was supported by CIHR grants FDN143343 (to DD), FDN143277 (to FS) and MOP81294 (to JLR), and a Grant-in-Aid from the Krembil Foundation (to DD).

Author contributions

MDW, FS and DD initiated the project. MDW assembled protein complexes and performed biochemical assays. SB and MDW performed cryo-EM and image analysis. AFT helped with biochemical assays. AS performed cellular assays. JPJ supervised bio-layer interferometry assays. AM performed molecular biology. SMN identified in vitro-ubiquitylated peptides. DD supervised the biochemical and cellular experiments and JLR supervised the cryo-EM experiments. MDW, FS, JLR and DD wrote the manuscript with input from the other authors.

Author Information:

Model coordinates for the NCP-ubme/53BP1 UDR structure are deposited in the Protein Data Bank under accession code 5KGF. Cryo-EM maps for NCP-ubme and NCP-ubme/GST-53BP1 are available at the EMDB under codes EMD-8247 and EMD-8246, respectively. Reprints and permissions information is available at www.nature.com/reprints. The authors declare no competing financial interests. Correspondence and requests for materials should be addressed to DD (durocher@lunenfeld.ca), JLR (john.rubinstein@utoronto.ca) or FS (sicheri@lunenfeld.ca).

Figure Legends

Figure 1. Architecture of the NCP-ubme/GST-53BP1 complex.

a, SEC-MALS performed on preformed NCP-ubme/GST-53BP1 complex compared to NCP-ubme or GST-53BP1 alone. **b**, 3D cryo-EM map of the NCP-ubme/GST-53BP1 complex. The map was segmented and colored according to the respective components. Weaker density corresponding to the tandem Tudor domain is displayed at a lower threshold. **c**, Model of the NCP-ubme/GST-53BP1 complex. **d**, Secondary structure model and sequence of the UDR region. Sites of NCP and ubiquitin interaction are indicated. Amino acid conservation is indicated (white, poorly conserved; black, highly conserved).

Figure 2. The molecular basis of H2AK15ub recognition by 53BP1.

a, Overlay of the NCP-ubme and NCP-ubme/GST-53BP1 structures. The cyan density is displayed with a higher threshold. **b**, Equivalent sections through maps of NCP-ubme (left) and NCP-ubme/GST-53BP1 (right), colored according to local resolution estimates[30]. **c**, Enlarged view of the region above the H2A Lys-15 isopeptide bond with ubiquitin in both structures. **d**, (Left) ubiquitin interactions with the αC helix of H2B. (Right) Magnified view of the H2AK15ub isopeptide bond, with flanking Arg-finger DNA-interacting residues indicated.

Figure 3. Multivalent recognition of NCP-ubme by the 53BP1 UDR.

a, (Left) UDR-ubiquitin interaction interface. (Right) Enlarged view of UDR-acidic patch interaction site colored according to coulombic surface charge. **b**, Bio-layer interferometry traces of a single concentration GST-53BP1 variants binding to immobilized NCP-ubme. WT: wild-type GST-53BP1 protein. **c**, Immunofluorescence analysis of U2OS cells depleted of 53BP1 by siRNA and transfected with GFP-53BP1$_{1220\text{-}1631}$ variants, post-irradiation. A representative stained cell is shown. Scale bar = 5 μm. Quantification of the cells with more than 10 GFP (53BP1) foci colocalizing with γH2AX is shown as mean ± s.e.m. (*n*=4). **d**, Bio-layer interferometry traces of GST-53BP1 with NCP-ubme containing proposed UDR-interacting H2A/H2B variants. WT: wild-type histone proteins **e**, Bio-layer interferometry traces of proposed acidic patch-interacting GST-53BP1 UDR variants with NCP-ubme. NB: no detectable binding.

Figure 4. Flexible association of 53BP1 tandem Tudor domain with NCP-ubme.

a, Magnified view of GST-53BP1 tandem Tudor density over the methylated tail of histone H4. Structure of 53BP1$_{1484\text{-}1601}$/H4 peptide (PDB: 1IG0[11]) was fitted. **b**, Indicated sections through the NCP-ubme/GST-53BP1 structure (left), from the calculated map (middle); or colored according to resolution (right), scale bar = 25 Å. **c**, Bio-layer interferometry traces comparing GST-53BP1 I1617A binding to NCP-ubme or equal concentrations of H4K$_C$20 dimethylated or unmethylated

peptides. A single GST-53BP1 I1617A association concentration (2 μM) is shown. NB: no detectable binding.

References

1 Lukas, J., Lukas, C. & Bartek, J. More than just a focus: The chromatin response to DNA damage and its role in genome integrity maintenance. *Nat Cell Biol* **13**, 1161-1169, doi:10.1038/ncb2344 (2011).

2 Dantuma, N. P. & van Attikum, H. Spatiotemporal regulation of posttranslational modifications in the DNA damage response. *EMBO J* **35**, 6-23, doi:10.15252/embj.201592595 (2016).

3 Jackson, S. P. & Durocher, D. Regulation of DNA damage responses by ubiquitin and SUMO. *Mol Cell* **49**, 795-807, doi:10.1016/j.molcel.2013.01.017 (2013).

4 Thorslund, T. *et al.* Histone H1 couples initiation and amplification of ubiquitin signalling after DNA damage. *Nature* **527**, 389-393, doi:10.1038/nature15401 (2015).

5 Stewart, G. S. *et al.* The RIDDLE syndrome protein mediates a ubiquitin-dependent signaling cascade at sites of DNA damage. *Cell* **136**, 420-434, doi:10.1016/j.cell.2008.12.042 (2009).

6 Doil, C. *et al.* RNF168 binds and amplifies ubiquitin conjugates on damaged chromosomes to allow accumulation of repair proteins. *Cell* **136**, 435-446, doi:10.1016/j.cell.2008.12.041 (2009).

7 Mattiroli, F. *et al.* RNF168 ubiquitinates K13-15 on H2A/H2AX to drive DNA damage signaling. *Cell* **150**, 1182-1195, doi:10.1016/j.cell.2012.08.005 (2012).

8 Gatti, M. *et al.* A novel ubiquitin mark at the N-terminal tail of histone H2As targeted by RNF168 ubiquitin ligase. *Cell Cycle* **11**, 2538-2544, doi:10.4161/cc.20919 (2012).

9 Panier, S. & Boulton, S. J. Double-strand break repair: 53BP1 comes into focus. *Nat Rev Mol Cell Biol* **15**, 7-18, doi:10.1038/nrm3719 (2014).

10 Fradet-Turcotte, A. *et al.* 53BP1 is a reader of the DNA-damage-induced H2A Lys 15 ubiquitin mark. *Nature* **499**, 50-54, doi:10.1038/nature12318 (2013).

11 Botuyan, M. V. *et al.* Structural basis for the methylation state-specific recognition of histone H4-K20 by 53BP1 and Crb2 in DNA repair. *Cell* **127**, 1361-1373, doi:10.1016/j.cell.2006.10.043 (2006).

12 Simon, M. D. *et al.* The site-specific installation of methyl-lysine analogs into recombinant histones. *Cell* **128**, 1003-1012, doi:10.1016/j.cell.2006.12.041 (2007).

13 Mattiroli, F., Uckelmann, M., Sahtoe, D. D., van Dijk, W. J. & Sixma, T. K. The nucleosome acidic patch plays a critical role in RNF168-dependent

ubiquitination of histone H2A. *Nat Commun* **5**, 3291, doi:10.1038/ncomms4291 (2014).
14 Vasudevan, D., Chua, E. Y. & Davey, C. A. Crystal structures of nucleosome core particles containing the '601' strong positioning sequence. *J Mol Biol* **403**, 1-10, doi:10.1016/j.jmb.2010.08.039 (2010).
15 McGinty, R. K., Henrici, R. C. & Tan, S. Crystal structure of the PRC1 ubiquitylation module bound to the nucleosome. *Nature* **514**, 591-596, doi:10.1038/nature13890 (2014).
16 Armache, K. J., Garlick, J. D., Canzio, D., Narlikar, G. J. & Kingston, R. E. Structural basis of silencing: Sir3 BAH domain in complex with a nucleosome at 3.0 A resolution. *Science* **334**, 977-982, doi:10.1126/science.1210915 (2011).
17 Arnaudo, N. *et al.* The N-terminal acetylation of Sir3 stabilizes its binding to the nucleosome core particle. *Nat Struct Mol Biol* **20**, 1119-1121, doi:10.1038/nsmb.2641 (2013).
18 Makde, R. D., England, J. R., Yennawar, H. P. & Tan, S. Structure of RCC1 chromatin factor bound to the nucleosome core particle. *Nature* **467**, 562-566, doi:10.1038/nature09321 (2010).
19 Barbera, A. J. *et al.* The nucleosomal surface as a docking station for Kaposi's sarcoma herpesvirus LANA. *Science* **311**, 856-861, doi:10.1126/science.1120541 (2006).
20 Davey, C. A., Sargent, D. F., Luger, K., Maeder, A. W. & Richmond, T. J. Solvent mediated interactions in the structure of the nucleosome core particle at 1.9 a resolution. *J Mol Biol* **319**, 1097-1113, doi:10.1016/S0022-2836(02)00386-8 (2002).
21 Long, L., Furgason, M. & Yao, T. Generation of nonhydrolyzable ubiquitin-histone mimics. *Methods* **70**, 134-138, doi:10.1016/j.ymeth.2014.07.006 (2014).
22 Baarends, W. M. *et al.* Increased phosphorylation and dimethylation of XY body histones in the Hr6b-knockout mouse is associated with derepression of the X chromosome. *J Cell Sci* **120**, 1841-1851, doi:10.1242/jcs.03451 (2007).
23 Pavri, R. *et al.* Histone H2B monoubiquitination functions cooperatively with FACT to regulate elongation by RNA polymerase II. *Cell* **125**, 703-717, doi:10.1016/j.cell.2006.04.029 (2006).
24 Nakamura, K. *et al.* Regulation of homologous recombination by RNF20-dependent H2B ubiquitination. *Mol Cell* **41**, 515-528, doi:10.1016/j.molcel.2011.02.002 (2011).
25 Zeng, M. *et al.* CRL4(Wdr70) regulates H2B monoubiquitination and facilitates Exo1-dependent resection. *Nat Commun* **7**, 11364, doi:10.1038/ncomms11364 (2016).
26 Iwasaki, W. *et al.* Comprehensive structural analysis of mutant nucleosomes containing lysine to glutamine (KQ) substitutions in the H3 and H4 histone-fold domains. *Biochemistry* **50**, 7822-7832, doi:10.1021/bi201021h (2011).

27 Leung, J. W. *et al.* Nucleosome acidic patch promotes RNF168- and RING1B/BMI1-dependent H2AX and H2A ubiquitination and DNA damage signaling. *PLoS Genet* **10**, e1004178, doi:10.1371/journal.pgen.1004178 (2014).
28 M.T. Morgan, M. H.-Y., A.E. Ringel, P. Bandi, A. Brik, C. Wolberger, . Structural basis for histone H2B deubiquitination by the SAGA DUB module. . *Science* **351**, 725-728 (2016).
29 Adkins, N. L., Niu, H., Sung, P. & Peterson, C. L. Nucleosome dynamics regulates DNA processing. *Nat Struct Mol Biol* **20**, 836-842, doi:10.1038/nsmb.2585 (2013).
30 Kucukelbir, A., Sigworth, F. J. & Tagare, H. D. Quantifying the local resolution of cryo-EM density maps. *Nat Methods* **11**, 63-65, doi:10.1038/nmeth.2727 (2014).

METHODS

Plasmids

Bacterial expression vectors of *Xenopus laevis* histone H3, H3 C110A and H4K20C are described in ref[10]. pET28a Synthetic Human H2A.1 and pET28a Human H2B.1 was a gift from Joe Landry (Addgene plasmids # 42634 and 42630, respectively). Expression plasmids for HisTEV-ub pProEx-6×His-TEV-Ubiquitin and HisTEV-ub G76C pProEx-6×His-TEV-Ubiquitin G76C were described in refs[10,31]. Plasmids encoding UBA1, UbcH5a and $RNF168_{1-113}$ and pcDNA5-NLS-GFP-$53BP1_{1220-1631}$ were described previously[10]. pUC57-8×145bp Widom-601 was a gift of Curt Davey, Nanyang Technical University.

The human 53BP1 DNA sequence corresponding to residues 1220-1631 was codon-optimized for bacterial expression by GeneArt (ThermoFisher). The native recruitment region, $53BP1_{1220-1631}$ was amplified and cloned into a modified pETM-30-02 GST-TEV vector described in ref[10]. DNA for the tandem Tudor and UDR segment of 53BP1 (corresponding to residues 1484-1631) was amplified from the codon optimized sequence by PCR and inserted into a modified pET24b, GST-expressing vector with a C-terminal 6×His tag, creating the GST-53BP1 expression vector. All mutations described in the manuscript were introduced by site directed mutagenesis (Quickchange; Stratagene), or via direct DNA synthesis in gBlocks (IDT Technologies) and subsequent sub-cloning. All plasmids were sequenced for verification.

Protein production

RNF168$_{1-113}$, UbcH5a, and Uba1 were expressed and purified as described previously[10]. In order to remove the 6×His tag from RNF168$_{1-113}$ and UbcH5a, the pure proteins were cleaved with 6×His-TEV protease at room temperature for 4 h in TEV cleavage buffer (50mM Tris-Cl pH 8, 150mM NaCl, 2mM Na-Citrate, 4 mM β-mercaptoethanol) and Ni^{2+} affinity subtracted (HiTrap chelating resin, GE healthcare) to remove 6×His-TEV protease and uncleaved 6×His tagged protein. Recombinant histones were purified essentially as described[32].

GST-53BP1 was produced in *E. coli* BL-21 DE3 CodonPlus cells, after inducing with 200 µM isopropyl β-D-1-thiogalactopyranoside (IPTG) for 18 h at 16 ^{o}C. Cells were lysed by sonication and lysozyme treatment in 1×Recom buffer (25 mM Na-phosphate buffer pH 7.4, 300 mM NaCl, 0.1% Triton (v/v), 10% glycerol (v/v), 4 mM β-mercapthoethanol, 1× Protease Inhibitor mix [284 ng/ml leupeptin, 1.37 µg/ml pepstatin A, 170 µg/ml phenylmethylsulfonyl fluoride and 330 µg/ml benzamindine], 5 µg/ml DNaseI). Clarified lysate was applied to a column of Fast-Flow Glutathione Sepharose (GE healthcare). After extensive washing in high (350 mM NaCl) and low (50 mM NaCl) salt buffers the protein was eluted with 25 mM reduced glutathione in 25 mM Tris-Cl pH 8, 150 mM NaCl, 10% glycerol (v/v), 4 mM β-mercaptoethanol. The eluate was concentrated with a 30K MWCO centrifugation device (Amicon) and further purified on either S200 10/300 (GE Healthcare) or SEC650 Enrich (BioRad) gel filtration columns in GF buffer (25 mM Tris-Cl pH 7.5, 125 mM NaCl, 2 mM DTT, 5% glycerol (v/v)). All GST-53BP1 variants, including Tudor, UDR mutants and GST-34-53BP1,

eluted primarily as dimeric species on size exclusion chromatography. Protein-containing fractions were concentrated, flash frozen in liquid nitrogen and stored at -80 ^{o}C. For Isothermal titration calorimetry (ITC) experiments proteins were dialyzed extensively into ITC buffer (20 mM HEPES pH 7.5, 200 mM KCl, 2 mM tris(2-carboxyethyl)phosphine (TCEP), 0.5 mM EDTA).

53BP1$_{1220-1631}$ was purified by glutathione affinity chromatography as described above. GST-TEV-53BP1$_{1220-1631}$ was cleaved from the resin overnight using TEV protease cleavage in TEV cleavage buffer. The eluate was concentrated with a 30K MWCO centrifugation device (Amicon) and further purified on a SEC650 Enrich (BioRad) gel filtration columns in GF buffer. Multiple peaks containing primarily 53BP1$_{1220-1631}$ were observed. The main protein containing peak was collected, concentrated, flash frozen in liquid nitrogen and stored at -80 ^{o}C.

HisTEV-ub variants were produced in *E. coli* BL-21 DE3 CodonPlus cells. lysed in 1×Recom buffer, with the NaCl adjusted to 500 mM. Clarified cell lysate was loaded onto a HiTrap chelating column (GE Healthcare) pre-loaded with Ni^{2+} ions. After extensive washing HisTEV-ub was eluted using a gradient of imidazole and peak-protein containing fractions were concentrated using a 3K MWCO centrifugation device (Amicon). HisTEV-ub was further purified on a S75 10/300 column in GF buffer. Protein-containing fractions were either concentrated by centrifugation or dialyzed into water supplemented with 1 mM acetic acid prior to lyophilization.

All protein concentrations were determined via absorbance at 280 nm using a Nanodrop 8000 (Thermo Scientific), followed by SDS-PAGE and InstantBlue (Expedeon) staining with comparison to known amounts of control proteins.

H4K$_C$20 labeling

Cysteine-engineered histone H4 K20C protein was alkylated essentially as described [12,33]. Briefly pure histone H4 was reduced with DTT prior to addition of a 50-fold molar excess of (2-chloroethyl) dimethylammonium chloride (Sigma-Aldrich). The reaction was allowed to proceed for 4 h at room temperature before quenching with 5 mM β-mercaptoethanol. The H4 protein was separated and desalted using a PD-10 desalting column (GE Healthcare) pre-equilibrated in water supplemented with 2 mM β-mercaptoethanol and lyophilized. Correct incorporation of alkylation agents was assessed by 1D intact weight ESI mass spectrometry (AIMS, Department of Chemistry, University of Toronto; see Extended Data Fig. 1b, further details below).

Catalytic ubiquitylation of H2A

H2A was ubiquitylated within a H2A-H2B dimer, the minimal complex required for K15 specificity[13]. The ubiquitylation reaction was performed in ubiquitylation reaction buffer (50 mM Tris-Cl pH 7.5, 120 mM NaCl, 5 mM $MgCl_2$, 1 μM $ZnCl_2$, 5 mM ATP, 1 mM DTT) with 120 nM Uba1 (E1), 500 nM UbcH5a (E2), 500 nM RNF168$_{1-113}$ (E3), 12.5 μM HisTEV-Ub and 4 μM H2A-H2B at 30 ^{o}C for 90 min.

The reaction was stopped either by addition of SDS loading buffer or an equal volume of quench buffer (9 M urea, 20 mM Tris-Cl pH 8, 80 mM NaCl, 2 mM EDTA).

The large-scale preparation of catalytically ubiquitylated H2A (Ub-$H2A_{CAT}$) was purified via loading of the urea-quenched reaction mix on a HiTrap SP column (GE Healthcare) using a peristaltic pump. The loaded column was connected to a FPLC (GE Healthcare) and washed with urea buffer A (7 M urea, 50 mM NaCl, 20 mM Tris-Cl pH 6.8, 2 mM β-mercaptoethanol) and bound histones were eluted using a gradient of urea buffer B (7 M Urea, 1 M NaCl, 20 mM Tris-Cl pH 8.8, 2 mM β-mercaptoethanol). HisTEV-H2AK15ub containing fractions were pooled and enriched over a HiTrap chelating column (GE Healthcare) pre-loaded with Ni^{2+} ions. Extensive washing in urea Ni^{2+} buffer (5.6 M urea, 20 mM Tris-Cl pH 8, 400 mM NaCl, 15 mM imidazole, 2 mM β-mercaptoethanol) removed non-specifically bound unmodified histones. HisTEV-H2AK15ub was eluted in Urea Ni^{2+} buffer, supplemented with 300 mM Imidazole. The Ni^{2+} column eluate was diluted to a final concentration of 1M urea, 200 mM NaCl and 55 mM imidazole and the 6×His tag at the N terminus of ubiquitin was removed by TEV cleavage overnight at 4 ^{o}C. TEV protease and uncleaved HisTEV-H2AK15ub was removed by Ni^{2+} subtraction and the resulting flow through was dialyzed extensively in water containing 2 mM β-mercaptoethanol, prior to lyophilization. H2AK15ub was refolded into histone octamers at an equimolar ratio to the other core histones, essentially as described[32].

Chemical ubiquitylation of H2A

Mutant H2A engineered with one cross-linkable cysteine (H2A K15C) was ubiquitylated by cross-linking alkylation, essentially as described[21,34], with the following modifications. H2A K15C (final concentration 700 μM) was incubated with HisTEV-ub G76C (final concentration 350 μM) in 250 mM Tris-Cl pH 8.6, 8 M urea and reduced with 5 mM TCEP (Sigma-Aldrich) for 30 min at room temperature. The bi-reactive cysteine cross-linker, 1,2-dibromoacetone (DBA, Santa Cruz), was dissolved in dimethyl formamide (DMF) and added to the protein mix to a final concentration of 4.2 mM. The reaction was allowed to proceed on ice for 1 h before quenching with 5 mM β-mercaptoethanol and reducing the pH to 8 with trifluoracetic acid (TFA). Chemically ubiquitylated H2A ($H2AK_C15ub$) was purified as described for the catalytic H2A ubiquitylation (see also Extended Data Fig. 5 a-c). $H2AK_C15ub$ was refolded into histone octamers at an equimolar ratio to the other core histones, essentially as described[32].

Nucleosome reconstitution

Nucleosome core particles (NCPs) were reconstituted essentially as described[10,32]. Briefly, the four core histones (with or without modifications) were resuspended in a guanidine hydrochloride denaturing buffer (20 mM Tris-Cl pH 7.5, 7 M guanidine-HCl, 10 mM DTT), mixed at equimolar ratios and then dialyzed into a refolding buffer (15 mM Tris-Cl pH 7.5, 2 M NaCl, 1 mM EDTA, 5 mM β-mercaptoethanol) to promote folding into a histone octamer. Correctly

folded octameric histones complexes were isolated by size exclusion chromatography on a S200 GL 10/300 (GE Healthcare).

Large-scale quantities of pUC57 8×145 Widom-601 DNA were isolated using multiple rounds of MaxiPrep kit purifications (Qiagen). Widom 601 145 bp DNA was purified as described[32] from the pUC57 8×145 601 sequence using EcoRV restriction enzyme to digest the DNA into fragments. Octamers were wrapped using a gradient dialysis technique with Widom-601 145bp DNA in Rb-low buffer (10 mM Tris-Cl pH 7.5, 200 mM KCl, 1 mM EDTA, 1 mM DTT). Proper assembly of wrapped NCPs, including all H2A and H2B mutants, was analyzed by native PAGE as described[32] and stained with SYBR Green dye (ThermoFisher, for example see Extended Data Fig. 1h). For gel source data, see Supplemental Fig. 1. NCP-ubme was further purified by differential PEG precipitation[17], by incubation with 5% (w/v) PEG-6000 for 10 min on ice, followed by centrifugation at 10,000×*g* at 4 °C for 10 minutes. The resulting pellet was resuspended in Rb-low buffer.

53BP1-NCP-ubme complex formation

A complex of GST-53BP1 and NCP-ubme was created by incubating the constituent reagents at a 2.5:1 molar ratio. The complex was purified by differential PEG precipitation, essentially as described[17]. Briefly, NCP-ubme (final concentration 20 μM) was incubated with GST-53BP1 (final concentration 50 μM) for 10 min on ice. PEG-6000 was added to a final concentration of 5% (w/v) and a precipitate allowed to form for 10 min on ice. The PEG precipitate was

centrifuged at 10,000×*g* for 10 min. The NCP-ubme/GST-53BP1 pellet was resuspended in Rb-low buffer and loaded onto a SEC650 Enrich (BioRad) gel filtration column, pre-equilibrated in Rb-low buffer. Fractions eluting earlier than NCP-ubme and GST-53BP1 alone were concentrated to >5 mg/ml and stored at 4 ^{o}C for downstream analysis.

Size exclusion chromatography Multi-angle light scattering (SEC-MALS)

SEC-MALS was performed on a Wyatt DAWN TREOS device connected to an Agilent Affinity FPLC using a 30NS prepacked column (Wyatt). The column was pre-equilibrated in Rb-low buffer and 80 µl of 15 µM of protein solution (either NCP-ubme, GST-53BP1 or NCP-ubme/GST-53BP1) was autoloaded onto the column. Data processing was performed using ASTRA software (Wyatt).

Isothermal titration calorimetry (ITC)

ITC measurements were performed on a microCal ITC-200 (GE Healthcare) at 13 ^{o}C. Prior to the experiment all proteins were extensively dialyzed against ITC buffer (20 mM HEPES pH 7.5, 200 mM KCl, 2 mM TCEP, 0.5 mM EDTA). The cell initially contained ~200 µl of NCP-ubme (H2AK$_{C}$15ub) at a concentration of 23.5 µM in ITC buffer. GST-53BP1 was added to the syringe at a concentration of 329 µM (i.e. 14 fold molar excess of the NCP-ubme cell concentration) and the protein was delivered as two injections of 0.5 µl, followed by 24 injections of 1.5 µl, with 3-min intervals between injections. Control experiments were performed under identical conditions to determine enthalpy changes occurring in the cell upon addition of GST-53BP1 to buffer alone. Curve fitting was performed in

Origin 7 software (GE Healthcare), using a standard one-site binding model and using the final four data points for baseline subtraction.

Biotin-labeling of NCP-ubme

NCP-ubme complexes were labeled on random surface lysines with biotin by using a 1:2 ratio of NCP to EZ-Link NHS-PEG4-Biotin (Thermo-Scientific) in labeling buffer (20 mM HEPES pH 8, 150 mM NaCl, 1 mM DTT, 0.5 mM EDTA). The mixture was incubated for 1 h at room temperature, before buffer exchange in Rb-low to remove unreacted NHS ester using Zeba spin 7K desalting columns (Thermo Scientific). The extent of biotinylation was assessed by binding to streptavidin biosensors (Pall ForteBio), and equal response levels of loading were used in all experiments. Biotinylation did not measurably disassemble NCPs or effect binding to GST-53BP1 (Extended Data Fig. 1h and data not shown).

Bio-layer interferometry (Octet) assays

Biotinylated NCPs or biotinylated H4 peptides were immobilized on streptavidin biosensors, until reaching a threshold binding of 0.8 nm or 1.5 nm (1.5 nm used for Figure 4c only), using an Octet RED96 system (Pall ForteBio). Streptavidin biosensors (Pall ForteBio) were pre-equilibrated in Modified Kinetics buffer (1× phospho-buffered saline [PBS], 0.025% Tween-20 (v/v), 0.02 % [BSA] (w/v), 0.1 mM DTT) for 10 min at room temperature. Experiments were set up in 96 well tray format, using a common protocol: 60 s equilibration in Modified Kinetics

buffer, loading of NCP/peptide to threshold value, 60 s wash in Modified Kinetics buffer, 180 s association in GST-53BP1 ligand solution matched to Modified Kinetics buffer, followed by 180 s dissociation in Modified Kinetics buffer. Trays were shaken at 1000 rpm during the experiment and all experiments were performed at 30 ^{o}C. Pilot experiments were performed for NCP-ubme and GST-53BP1 mutants to determine the optimal concentrations for kinetic analysis. The assay was performed on four identically loaded sensors, dipped into four wells with consecutive 2-fold dilutions of ligand (GST-53BP1 variants of 53BP1$_{1220-1631}$). All dilutions were prepared in Modified Kinetics buffer.

All data were normalized to baseline and subtracted from minimal non-specific binding, based on a blank sensor incubated with the highest concentration of ligand. All data were analyzed in Forte Bio Octet analysis software. Full binding kinetics experiments showed a dose-response behavior correlated with dilution series. Due to the biological complexity of 53BP1 binding to NCP-ubme full kinetic fitting was not possible. All experiments were repeated at two immobilization densities, with similar results obtained. Plots of a single ligand concentration (0.5 μM GST-53BP1 variants in all figures except Fig. 4c) were prepared in Prism (GraphPad). Fold differences of mutants compared to wild-type were determined at a single time point (180 s) across multiple different GST-53BP1 variant concentrations, in the association portion of the binding event.

NCP pull-down assays

Pull-down assays were performed essentially as described[10]. Briefly, 4 µg of GST-tagged 53BP1 constructs were immobilized on glutathione-sepharose resin (GE Healthcare), before incubation with 2.2 µg of NCP complex in Pull-down buffer (50 mM Tris-Cl pH 7.5, 150 mM NaCl, 1 mM DTT, 0.05% NP-40 (v/v), 0.1% (w/v) BSA). Pull-downs were washed thoroughly in pull-down buffer and resuspended directly in 2× SDS loading buffer. For the LANA peptide competition assay, the pull-down was performed as normal, with the addition of LANA peptide during the incubation with NCP. All pull-down assays were repeated two times, with a single Immunoblot displayed.

Immunoblotting

Proteins were separated by SDS-PAGE and transferred to nitrocellulose membranes. All blocking and anibody incubations were performed in Tris-buffered saline containing either 5% (w/v) BSA or 5% (w/v) skimmed milk powder. For Western blotting the following commercial primary antibodies were used: rabbit anti-H2B (Abcam), rabbit anti-H3 (Abcam), rabbit anti-GST (Santa Cruz). A rabbit polyclonal H2A antibody was raised against a peptide encompassing human H2A residues 100-130 (KVTIAQGGVLPNIQAVLLPKKTESHHKAKGK) coupled to KLH (Covance). Serum from a single immunized mouse serum was found to specifically recognize histone H2A (validation of the antibody is the Supplementary information figure 2). HRP-conjugated goat anti-rabbit IgG (Jackson

Immunoresearch) secondary antibodies were used with enhanced chemiluminescence solution (ECL supersignal, Thermo Scientific) was used for protein detection. All pull-down assays were repeated two times, with a single Immunoblot displayed. For gel source data, see Supplemental Fig. 1.

Protein cross-linking

NCP-ubme with H2B cysteine mutations (N84C or E105C) were assembled as previously described, except using a H3 where the sole native cysteine was mutated (H3 C110A). NCPs were desalted using Zeba spin desalting columns (Thermo Scientific) to remove reducing agents into degassed cross-linking buffer (20 mM Tris-Cl pH 8, 100 mM NaCl, 1 mM EDTA). NCPs were then incubated in a 1:5 ratio with the bifunctional maleimide bismaleimidoethane (BMOE) for 1 h at room temperature. BMOE-conjugated NCPs were again desalted and quantified. A final concentration of 1.5 µM BMOE-NCP-ubme was mixed with a 6-fold molar excess of freshly desalted GST-53BP1 cysteine mutants (T1609C or K1628C). The reaction was incubated for 2 h at room temperature and quenched by addition of SDS loading buffer supplemented with 25 mM β-mercaptoethanol. The extent of crosslinking was assessed by immunoblotting with anti-H2B antibodies.

Mass spectrometry

In vitro ubiquitylation reaction products of H2A and H2B (4 µg of each) were separated on a 15% SDS-PAGE gel and bands were excised at the height of the

non-modified, mono- and di-ub forms (based on molecular size markers run in parallel). Proteins were in-gel digested at 37 °C for 330 min using 100ng trypsin (Worthington) and gel extracted using TFA-acidification and acetonitrile dehydration. Peptides were cleaned up using C18 stage tips (Thermo Scientific) and dried to completeness. Peptides were reconstituted in 5 % (v/v) formic acid and loaded onto a 12 cm fused silica column with a pulled tip that was packed in-house with 3.5 µm Zorbax C18 (Agilent Technologies). Samples were analyzed using an Orbitrap Elite (Thermo Scientific) coupled to an Eksigent nanoLC ultra (AB SCIEX). Peptides were eluted from the column using a 90 min linear gradient from 2 % to 35 % (v/v) acetonitrile in 0.1 % (v/v) formic acid. Tandem MS spectra were acquired in a data-dependent mode for the top 10 most abundant multiply charged peptides, with a dynamic exclusion duration of 20 s. Tandem MS spectra were acquired using Collision induced dissociation. Mascot was used to search spectra against the human Refseq_V53 database, allowing up to two missed cleavages and including GlyGly (K) and LeuArgGlyGly (K) as variable modifications. Fragmentation spectra of diGly-peptides identified by Mascot were manually verified.

Determination of the intact mass of histone H4 peptides and H4 protein was performed at AIMS Mass Spectrometry facility, Department of Chemistry, University of Toronto. Electrospray ionization (ESI) mass spectra were acquired in positive ion mode using a 6538 UHD model quadrupole time-of-flight mass spectrometer equipped with a 1260 Infinity Series HPLC (Agilent Technologies, Santa Clara, CA). Intact proteins were mass analyzed following online de-salting

using a Tricorn 5/50 column packed with Sephadex G-25 size-exclusion media (GE Healthcare). The mobile phase was 1:1 (v/v) 0.1 % aqueous formic acid: methanol, flowing at a rate of 500 µl/min. Samples were diluted in mobile phase to a concentration of approximately 0.1 µM and injections on the column were 2.5 µl.

Peptides

The wild-type $LANA_{1-23}$ peptide (Biotin-LC-MAPPGMRLRSGRSTGAPLTRGSY), the non-binding $LANA_{1-23}$ 8LRS10 (Biotin-LC-MAPPGMRAAAGRSTGAPLTRGSY) and the biotinylated $H4K20C_{12-27}$ peptide (Biotin-LC-KGGAKRHRCVLRDNIQ) were synthesized by BioBasic. Peptides were modified to create dimethyl-lysine analogs (using (2-chloroethyl)-dimethylammonium chloride [Sigma-Aldrich]) or lysine analogs (using (2-bromoethyl)-ammonium bromide [Millipore]) as described for histone H4. Peptides were purified from the reactant materials by SepPak C18 columns (Cell Signaling) and lyophilized dry, before resuspension in DMSO for downstream assays. Correct incorporation of alkylation agents was assessed by intact weight ESI Mass spectrometry (AIMS, Chemistry Department, University of Toronto, Extended Data Fig. 10bc)

Cryo-EM grid preparation and microscopy

Holey carbon film-coated EM grids were prepared with arrays of 500-800 nm holes by nanofabrication[35]. 2.5 µl of NCP-ubme or NCP-ubme/GST-53BP1

complex was diluted to a final salt concentration of ~50 mM. The low-salt complexes were applied to grids and allowed to equilibrate for 5 s in a FEI Vitrobot grid preparation robot, and blotted from both sides for 15 s prior to freezing in a liquid ethane/propane mixture (1:1 v/v) mix[36]. Grids were subsequently stored in liquid nitrogen, prior to transfer to a Gatan 626 cryotransfer specimen holder. Samples were imaged with a FEI F20 electron microscope, equipped with a field emission gun and operating at 200 kV. Movies were acquired with a Gatan K2 Summit direct detector device (DDD) camera using a calibrated magnification of 34,483×, resulting in a physical pixel corresponding to 1.45 Å. The DDD was used in counting movie mode with 5 electrons/pixel/s for 15 s and 0.5 s/frame. This exposure rate resulted in 1.2 electrons/Å^2/frame and a total exposure of 36 electrons/Å^2 on the specimen. A total number of 227 movies were acquired for the NCP-ubme with a defocus range from 1 to 3.2 μm. 319 movies were acquired for the NCP-ubme/GST-53BP1 with defocus between 0.8 and 4.1 μm. NCP-ubme and NCP-ubme/GST-53BP1 datasets were treated similarly.

Cryo-EM image analysis

Individual frames in a movie stack were aligned and averaged using the programs alignframes_lmbfgs and shiftframes[37]. Contrast transfer function (CTF) parameters were calculated from the averaged frames using CTFFIND3[38]. Manual inspection of micrographs and their corresponding power spectra was performed in Relion 1.3[39] and undesirable micrographs were discarded due to

contamination or lack of high resolution Thon rings in their power spectrum. Automatic particle picking, based on manually selected templates, was performed in Relion 1.3. After particle extraction, beam induced particle motion between frames was corrected with alignparts_lmbfgs[37]. A previously measured 2% magnification anisotropy was corrected as described[40]. Extracted particles were subject to 2D classification in Relion 1.3 and classes with averages that resembled the expected projections of NCPs were selected for 3D classification. A low pass filtered model of NCP based on PDB: 1KX5[20] was used as a template for 3D classification into 9 classes (NCP-ubme/GST-53BP1) or 4 classes (NCP-ubme). Particle images from 3D classes that showed high-resolution features were refined further. Refined maps of NCP-ubme/GST-53BP1 were sharpened in Relion 1.3 with an automatically determined B-factor. NCP-ubme maps were not sharpened. Global resolution estimates were determined using the FSC=0.143 criterion after a gold-standard refinement[41]. Local resolution was estimated with ResMap[30]. Calculations with Relion 1.3 were performed using the SickKids High Performance Facility (Hospital for Sick Children, Toronto). All programs utilized are freely available through the respective cited distributors.

Structure editing and modeling

The atomic models of Widom-601 DNA (PDB: 3LZ0[14]), octameric histones (PDB: 1KX5[20]), ubiquitin (PDB: 1UBI[42]) and H4K20me2/53BP1 tandem Tudor domain (PDB: 2IG0[11]) were fitted in UCSF Chimera[43] without allowing flexibility into the 3D maps. Map segmentation was performed in UCSF Chimera. For the NCP-ubme structure the ubiquitin segmentation was further modified to remove

obvious NCP density from the ubiquitin segment. In Figure 2a density corresponding to ubiquitin in the NCP-ubme structure was displayed with a threshold of 0.125. The rest of the NCP-ubme and NCP-ubme/GST-53BP1 are displayed with a threshold of 0.29 and 0.395, respectively. The H2A/H2B sequence was mutated to the human H2AK13R/K36R and H2B manually in UCSF Chimera. A polyalanine model of the UDR was built within the UDR density in Coot[44], which compared well to predicted structures generated by Robetta[45]. The UDR model was mutated and fitted in UCSF Chimera, followed by iterative rounds of real-space refinement in PHENIX[46] and model optimization in Coot. All figures were prepared in UCSF Chimera.

Cell culture

U-2-OS (U2OS) cells were purchased from ATCC and verified mycoplasma free. Cells were cultured with McCoy's Medium (Gibco) supplemented with 10% fetal bovine serum and maintained at 37 ^{o}C in 5 % CO_2 atmosphere conditions. Knock-down by single duplex siRNA to 53BP1 (ThermoFisher, D-003548-01, target sequence: 5'-GAGAGCAGAUGAUCCUUUA-3') was performed with RNAiMAX (Invitrogen) two days prior to fixation, following the manufacturers' instructions. One day prior to fixation, cells were transiently transfected with the plasmid NLS-GFP-53BP1$_{1220-1631}$ DNA using Lipofectamine-3000 transfection reagent (Invitrogen).

Immunofluorescence Microscopy

One hour after exposure to 2 Gy of ionizing radiation cells were fixed with 4 % (w/v) formaldehyde. Fixed cells were permeabilized in PBS, 0.3% (v/v) Triton X-

100 and blocked in blocking buffer (PBS, 10% (v/v) goat serum, 0.5% (v/v) NP-40, 0.5% (w/v) Saponin). Cover-slips were stained with anti-γH2AX (Millipore) and anti-mouse IgG Alexa–fluor 647 (Millipore) secondary antibody. DNA was counterstained with DAPI, which was used to trace the outline of nuclei. Stained cells were visualized on a LSM780 Zeiss confocal microscope. Quantification was performed on 100 U2OS cells (N = 3), where a cell with > 10 GFP-53BP1 foci was considered positive.

Extended data

Extended data Figure 1. Generation of homogenously methylated and ubiquitylated NCPs.

a, Schematic of H4 cysteine alkylation to create a dimethyl-lysine analog. **b**, 1D intact mass spectra of the alkylated H4K$_C$20me2 protein after desalting and lyophilization. **c**, Mass spectrum of the identified off-target K36 ubiquitylation. Fragmentation spectrum of the 37-K(GlyGly)GNYAER-43 H2A peptide (476.237091 Da, 2^+ charge state, Mascot ions score: 45). This spectrum originates from di-ubiquitylated forms of *in vitro* ubiquitylated H2A that were separated by SDS-PAGE, subjected to limited trypsin digestion and analyzed by tandem mass spectrometry. **d**, Immunoblot analysis of a H2A-H2B dimer ubiquitylation reaction. Comparison of K13/15/36R triple mutated and K13/36R double mutated H2A variants using optimized conditions to minimize off-target ubiquitylation for large-scale reactions. **e**, SDS-PAGE analysis of the first step in H2AK15ub purification, cation exchange chromatography (In: input; FT: flow-through; W: wash; M: molecular weight marker). The ubiquitin is tagged with an N-terminal hexa-histidine tag and TEV cleavage site (termed HisTEV-ub). **f**, SDS-PAGE analysis of the second step in H2AK15ub purification, nickel ion affinity chromatography. **g**, SDS-PAGE analysis of TEV protease cleavage of HisTEV-H2AK15ub and subsequent nickel column depletion. Cleaved H2AK15ub flows through (Ni FT) the column, while uncleaved product and His-tagged TEV protease binds it (not shown). **h**, Native polyacrylamide gel analysis of wrapped NCPs. The gel was stained with SYBR Green to identify DNA. Wrapping of NCPs

results in quenching of the SYBR green signal and a shift in the electrophoretic mobility of the DNA. Ubiquitylated NCPs (H2A-ub) appear as a doublet, which runs higher than solely methylated NCPs (WT H2A). Biotinylation on NCP surface lysines, required for downstream bio-layer interferometry analysis, does not measurable effect migration in the gel (H2A-ub-Bio). WT: wild-type H2A protein.

Extended data Figure 2. Formation of NCP-ubme and NCP-ubme/GST-53BP1 complexes.

a, Schematic representation of full length human 53BP1, 53BP1 with the native recruitment region, 53BP1$_{1220\text{-}1631}$, and GST-53BP1$_{1484\text{-}1631}$ (termed GST-53BP1). 53BP1$_{1220\text{-}1631}$ and GST-53BP1 constructs are used throughout this manuscript. Identified domains are highlighted; oligo: oligomerisation domain. **b**, Pull-down assay of GST-53BP1 variants containing either the 16-residue linker used throughout this study or a longer 34-residue linker. The L1619A UDR mutant was included as a negative control. **c**, Bio-layer interferometry assays of GST-53BP1 or a native 53BP1$_{1220\text{-}1631}$ fragment. **d**, SDS-PAGE of purified 53BP1 proteins used in the pull-down and bio-layer interferometry assays. M: molecular weight markers. **e**, Isothermal titration calorimetry (ITC) measurement investigating the affinity of GST-53BP1 (syringe) to NCP-ubme (cell). Data reported as the mean +/- s.e.m. (*n*=2). **f**, SDS-PAGE analysis of NCP-ubme/GST-53BP1 complex formation by differential PEG precipitation[17] (In, input; S, soluble supernatant; P, pellet). An excess of GST-53BP1 was added,

which was not precipitated with the NCP-ubme. **g**, SDS-PAGE analysis of size exclusion chromatography fractions, isolating NCP-ubme/GST-53BP1. In, Input; M, size markers. Fractions 8-10 were pooled and used for SEC-MALS analysis (Fig. 1a) and subsequent structure determination.

Extended data Figure 3. Cryo-EM structure determination and validation of NCP-ubme/GST-53BP1 complex.

a, Representative cryo-EM micrograph of the NCP-ubme/GST-53BP1 complex. Example particle images in different orientations are boxed. **b**, Power spectrum from a representative micrograph showing Thon rings that extend beyond 7 Å resolution. **c**, Example particle images, scale bar corresponds to 25 Å. **d**, Examples of 2D class averages obtained during image processing of the NCPubme/GST-53BP1 complex (CTF corrected, inverted contrast), scale bar corresponds to 25 Å. **e**, Fourier shell correlation curve after a gold-standard map refinement. **f**, Euler angle distribution plot of all particles used for the symmetrized final map. Bar length and color (blue, low; red, high) corresponds to number of particle images contributing to each view. **g**, (Upper left) Magnified view of the H2B-H4 cleft with clear side chain density observed for H2B Arg-89, Gln-92 and Arg-96. (Upper right) Magnified view of the H2B αC helix and H2A α1 helix. Densities for aromatic side-chains of H2A Tyr-50, H2B Tyr-121 and the bulky residue H2A Arg-17 are visible. (Lower) Magnified view of the C terminus of the H2A α2 helix, with density for base of the side chain of Arg-71 visible. **h**, Schematic of predicted location of flexible GST moiety (green) used for 53BP1

dimerization (PDB: 1Y6E[47]). No cryo-EM density can be attributed to GST, suggesting that it is highly flexible between different particles in the population sampled. Dashed lines indicate the 16 amino acid linker region incorporated in the GST-53BP1 construct (black) and the flexible C-terminal tail of the GST (green). The linker peptide region could span up to ~80 Å, allowing significant flexibility of the GST dimers, shown here positioned ~50 Å from the N terminus of the modeled Tudor domain.

Extended data Figure 4. Cryo-EM structure determination and validation of NCP-ubme complex.

a, Surface rendering of the NCP-ubme complex, viewed along the DNA axis and the orthogonal direction. Density corresponding to ubiquitin was segmented, Gaussian filtered and displayed with a threshold of 0.125 (area within dashed line). The rest of the NCP-ubme is displayed with a threshold 0.35. Rigid body fitting of the high resolution structure of histone octamers (PDB: 1KX5[20]), Widom-601 145bp DNA (PDB: 3LZ0[14]) and ubiquitin (PDB: 1UBI[42]) into NCP-ubme density is shown. Ubiquitin could not be readily placed in the attributed density. **b**, Representative cryo-EM micrograph of the NCP-ubme complex. Example particle images showing different orientations are boxed. **c**, Power spectrum from a representative micrograph showing Thon rings. **d**, A selection of particles images after extraction from the dataset, scale bar corresponds to 25 Å. **e**, Examples of 2D class averages obtained during image processing (CTF corrected, inverted contrast), scale bar corresponds to 25 Å. **f**, Fourier shell

correlation curve after gold-standard map refinement. **g**, Euler angle distribution plot of all particle images used for the symmetrized final map. Bar length and color corresponds to number of particle images in each view that contributed to final 3D map (blue, low; red, high).

Extended data Figure 5. Chemical ubiquitylation of H2A and the constrained conformation of ubiquitin in the NCP-ubme/GST-53BP1 complex.

a, Schematic of cross-linking reaction scheme between an electrophilic acetone (dibromoacetone, DBA) and two engineered cysteine residues in H2A and ubiquitin, respectively. TCEP was added to initially reduce disulphide bonds. **b**, Pilot reactions of cross-linkable ubiquitin mixed with H2A. Cross-linked products were separated by SDS-PAGE. H2A-only and ubiquitin-only reactions identify non-productive cross-linking in the final reaction, H2A-H2A and ub-ub. Correctly modified H2A is labeled $H2AK_C15ub$. Hexahistadine and TEV consensus sequence-tagged ubiquitin was used (HisTEV-ub) **c**, Chemically ubiquitylated $H2AK_C15ub$-containing NCPs interact with GST-53BP1. Immunoblot (IB) analysis of GST-53BP1 pull-down (PD) using NCPs assembled with unmodified H2A, catalytically ubiquitylated H2A or chemically ubiquitylated H2A ($H2AK_C15ub$). In this pilot experiment, the chemically ubiquitylated H2A runs with lower mobility due to the retention of the HisTEV tag. The tag was removed in all future experiments. **d**, Space filling model of the covalently tethered ubiquitin, in a closed conformation, pulled over the surface of NCP. Key interacting histone

residues are labeled. **e**, Bio-layer interferometry traces of a single concentration of GST-53BP1 association and dissociation with immobilized NCP-ubme containing the indicated mutations in the H2B αC helix. Relative affinities are also shown. WT: wild-type H2B. **f**, Immunoblot analysis of GST-53BP1 pull-down assay to determine the effect of mutating the αC helix H2B residues that potentially form a hydrogen-bonding network with closed, 53BP1-bound ubiquitin. WT: wild-type H2B protein. **g**, Stained SDS-PAGE gel of purified reconstituted, nucleosomes used in this figure. (Left) H4K_C20me2-modified NCPs containing cross-linked ubiquitin at indicated residues in H2A, H2B or both. These NCPs were used in assays in panels **e** and **f**. (right) Biotinylated NCP-ubme complexes containing H2B variants used in the bio-layer interferometry assays. **h**, Immunoblot analysis of GST-53BP1 pull-down assay investigating the effect of H2BK120ub on GST-53BP1 binding to NCP-ubme.

Extended data Figure 6. Structural basis of 53BP1 specificity for H2AK15ub.

a, Diagrammatic representation of the arginine-fingers mechanism of 53BP1 recognition of H2AK15ub-containing NCPs. Sequences of H2A mutations are detailed in **c**. **b**, Top view of the H2A N-terminal tail, displaying the modeled arginines projecting into the nucleosomal DNA grooves. For clarity, only the DNA phosphodiester backbone is shown. **c**, Immunoblot analysis of pull-down (PD) assay with RNF168-ubiquitylated NCPs containing the indicated H2A variants detailed at the bottom. GST-53BP1 can recognize H2AK13ub only when

arginine-17 has been removed, allowing a shift in the N-terminal tail. Proposed R/KxxxKubxR consensus binding motif is indicated.

Extended data Figure 7. Specific orientation of the UDR region and H2B-H4 cleft interactions.

a, (Top) Schematic of 53BP1 UDR region, indicating sites of engineered cysteines used for BMOE cross-linking (purple arrowheads). (Bottom) Surface representation of modeled NCP with interaction interfaces colored; tandem Tudor domain (H4 tail: red), UDR (H2B/H4 cleft, H2B αC helix and acidic patch: yellow) and ubiquitin (H2B αC helix and H2AK15: purple). Locations of engineered H2B cysteine residues used for cross-linking are indicated (N84C and E105C). **b**, Immunoblot analysis of covalently cross-linked NCP-ubme-GST-53BP1 variants. BMOE, a bivalent maleimide cross-linker, was first reacted with NCP-ubme-containing H2B single cysteine variants, before incubation with cysteine cross-linkable GST-53BP1 variants. Cross-linking to H2B is visualized by a shift in apparent molecular weight, equivalent to the addition of one GST-53BP1 moiety. The relatively weaker cross-linking of H2BE105C and GST-53BP1K1628C probably arises from the fact that the lysine is predicted to interact on the other face of the acidic patch. The asterisk denotes a non-specific band due to cross-reactivity of the anti-H2A antibody with non cross-linked GST-53BP1. **c**, Magnified view of the H2B-H4 cleft at the rear of the NCP, with modeled UDR chain in the yellow density. Ribbon structure of Sir3 BAH domain (residues 75-83; PDB: 3TU4[16]), also proposed to interact in this region, was overlaid (purple).

Extended Data Figure 8. Validation of UDR-ubiquitin interaction.

a, Immunoblot analysis of pull-down (PD) assays, immobilizing the indicated GST-53BP1 UDR mutations in residues 1616-1620 and monitoring NCP-ubme interaction. WT: wild-type GST-53BP1 protein. **b**, SDS-PAGE of purified GST-53BP1 UDR proteins used in the pull-down and bio-layer interferometry assays. M: molecular weight markers. **c**, Pull-down assays (PD) of GST-53BP1 with the indicated NCP-ubme variants. **d**, Bio-layer interferometry traces of NCP-ubme prepared with the indicated ubiquitin variants chemically ligated to H2A at position 15. NB: No binding detected. **e**, SDS-PAGE analyses of reconstituted, biotinylated nucleosomes used in panel **f**, (Top) Enlarged view of the 53BP1-bound constrained modeled ubiquitin, with ball and stick representations of ubiquitin lysine residues indicated. Note the accessibility of Lys-27 and Lys-63, both reported to be following DSBs. (Bottom) Model of a Lys-63-linked di-ubiquitin (PDB: 3H7S[48]) built on H2AK15 within the NCPubme/GST-53BP1 structure. The distal ubiquitin (pink) projects away from the NCP surface towards the tandem Tudor domain of 53BP1, shown in orange. While we note a minor steric clash between the modeled distal ubiquitin and the tandem Tudor domain, we surmise that the inherent flexibility of ubiquitin chains, coupled with the flexibility of the tethered Tudor domain on the H4 tail, likely enables 53BP1 to bind to NCPs with Lys63-linked ubiquitin chains on H2AK15.

Extended Data Figure 9. 53BP1 UDR interactions with the nucleosome acidic patch.

a, Magnified view of a ribbon representation of the NCP-ubme acidic patch with the overlaying density attributed to the UDR. **b**, Immunoblot analysis of a GST-34-53BP1 pull-down (PD) assay performed with RNF168-ubiquitylated NCP-me, in the presence of the acidic patch-interacting LANA peptide (the GST-53BP1 protein used here has the 34 amino acid linker). The indicated amounts of LANA peptide were added as a competitor during the pull-down (concentration in μM). 8LRS10 peptide has negligible NCP binding[19] and used as a control. **c**, Immunoblot analysis of GST-53BP1 pull-downs (PD) using NCP-ubme incorporating the indicated H2A and H2B mutants, which localize to the acidic patch and adjacent H2B αC helix. **d**, SDS-PAGE and InstantBlue staining to analyze purified reconstituted, biotinylated nucleosomes containing H2A/H2B mutations used in the bio-layer interferometry assays. Compare to WT NCP-ubme in Extended Data Fig. 5g (right panel). **e**, Immunoblot analysis of GST-53BP1 pull-down assays, using selected 53BP1 UDR basic residue mutations. WT: wild-type GST-53BP1 protein. **f**, SDS-PAGE and InstantBlue staining to analyze purified GST-53BP1 UDR variant proteins used in the bio-layer interferometry assays in **Fig. 3e**. M: molecular weight markers. **g**, Enlarged view of UDR-acidic patch interaction site colored according to coulombic surface charge, overlaid with the structure of other acidic patch chromatin binding factors: KSHV LANA peptide (PDB: 1ZLA[19]); the Sir3 BAH domain (PDB: 3TU4[16]) and the PRC1 complex (PDB:4R8P[15]).

Extended Data Figure 10. Flexibility of the 53BP1 tandem Tudor domain in the NCP-ubme structure and comparison of GST-53BP1 to 53BP1$_{1220-1631}$.

a, A selection of aligned 3D maps obtained during determination of the NCP-ubme/GST-53BP1 structure, with an enlarged view of the density from the tandem Tudor domain of 53BP1, shown in the lower panels. Note that the position of the tandem Tudor domain density is highly variable, but is always tethered over the H4 N-terminal tail. **b**, 1D intact mass spectra of Biotin-LC-H4$_{12-27}$ K20C peptide chemically alkylated to create a lysine mimic. The reaction proceeded to near completion, but some unreacted peptide can be observed at 2190 Da. **c**, 1D intact mass spectra of Biotin-LC-H4$_{12-27}$ K20C, peptide chemically alkylated to create a dimethyl lysine mimic. The reaction proceeded to near completion, but some unreacted peptide can be observed at 2190 Da. **d**, Bio-layer interferometry traces comparing the binding of GST-53BP1 with 53BP1$_{1220-1631}$ to NCP-ubme variants. Data from a single 53BP1 protein concentration is plotted.

Extended References

31 Juang, Y. C. *et al.* OTUB1 co-opts Lys48-linked ubiquitin recognition to suppress E2 enzyme function. *Mol Cell* **45**, 384-397, doi:10.1016/j.molcel.2012.01.011 (2012).

32 Dyer, P. N. *et al.* Reconstitution of nucleosome core particles from recombinant histones and DNA. *Methods Enzymol* **375**, 23-44 (2004).

33 Simon, T. W. *et al.* The use of mode of action information in risk assessment: quantitative key events/dose-response framework for modeling the dose-response for key events. *Crit Rev Toxicol* **44 Suppl 3**, 17-43, doi:10.3109/10408444.2014.931925 (2014).

34 Orthwein, A. *et al.* A mechanism for the suppression of homologous recombination in G1 cells. *Nature* **528**, 422-426, doi:10.1038/nature16142 (2015).

35 Marr, C. R., Benlekbir, S. & Rubinstein, J. L. Fabrication of carbon films with approximately 500nm holes for cryo-EM with a direct detector device. *J Struct Biol* **185**, 42-47, doi:10.1016/j.jsb.2013.11.002 (2014).

36 Tivol, W. F., Briegel, A. & Jensen, G. J. An improved cryogen for plunge freezing. *Microsc Microanal* **14**, 375-379, doi:10.1017/S1431927608080781 (2008).

37 Rubinstein, J. L. & Brubaker, M. A. Alignment of cryo-EM movies of individual particles by optimization of image translations. *J Struct Biol* **192**, 188-195, doi:10.1016/j.jsb.2015.08.007 (2015).

38 Mindell, J. A. & Grigorieff, N. Accurate determination of local defocus and specimen tilt in electron microscopy. *J Struct Biol* **142**, 334-347 (2003).

39 Scheres, S. H. RELION: implementation of a Bayesian approach to cryo-EM structure determination. *J Struct Biol* **180**, 519-530, doi:10.1016/j.jsb.2012.09.006 (2012).

40 Zhao, J., Brubaker, M. A., Benlekbir, S. & Rubinstein, J. L. Description and comparison of algorithms for correcting anisotropic magnification in cryo-EM images. *J Struct Biol* **192**, 209-215, doi:10.1016/j.jsb.2015.06.014 (2015).

41 Rosenthal, P. B. & Henderson, R. Optimal determination of particle orientation, absolute hand, and contrast loss in single-particle electron cryomicroscopy. *J Mol Biol* **333**, 721-745 (2003).

42 Ramage, R. *et al.* Synthetic, structural and biological studies of the ubiquitin system: the total chemical synthesis of ubiquitin. *Biochem J* **299 (Pt 1)**, 151-158 (1994).

43 Pettersen, E. F. *et al.* UCSF Chimera--a visualization system for exploratory research and analysis. *J Comput Chem* **25**, 1605-1612, doi:10.1002/jcc.20084 (2004).

44 Emsley, P., Lohkamp, B., Scott, W. G. & Cowtan, K. Features and development of Coot. *Acta Crystallogr D Biol Crystallogr* **66**, 486-501, doi:10.1107/S0907444910007493 (2010).

45 Kim, D. E., Chivian, D. & Baker, D. Protein structure prediction and analysis using the Robetta server. *Nucleic Acids Res* **32**, W526-531, doi:10.1093/nar/gkh468 (2004).
46 Adams, P. D. *et al.* PHENIX: a comprehensive Python-based system for macromolecular structure solution. *Acta Crystallogr D Biol Crystallogr* **66**, 213-221, doi:10.1107/S0907444909052925 (2010).
47 Rufer, A. C., Thiebach, L., Baer, K., Klein, H. W. & Hennig, M. X-ray structure of glutathione S-transferase from Schistosoma japonicum in a new crystal form reveals flexibility of the substrate-binding site. *Acta Crystallogr Sect F Struct Biol Cryst Commun* **61**, 263-265, doi:10.1107/S1744309105004823 (2005).
48 Weeks, S. D., Grasty, K. C., Hernandez-Cuebas, L. & Loll, P. J. Crystal structures of Lys-63-linked tri- and di-ubiquitin reveal a highly extended chain architecture. *Proteins* **77**, 753-759, doi:10.1002/prot.22568 (2009).

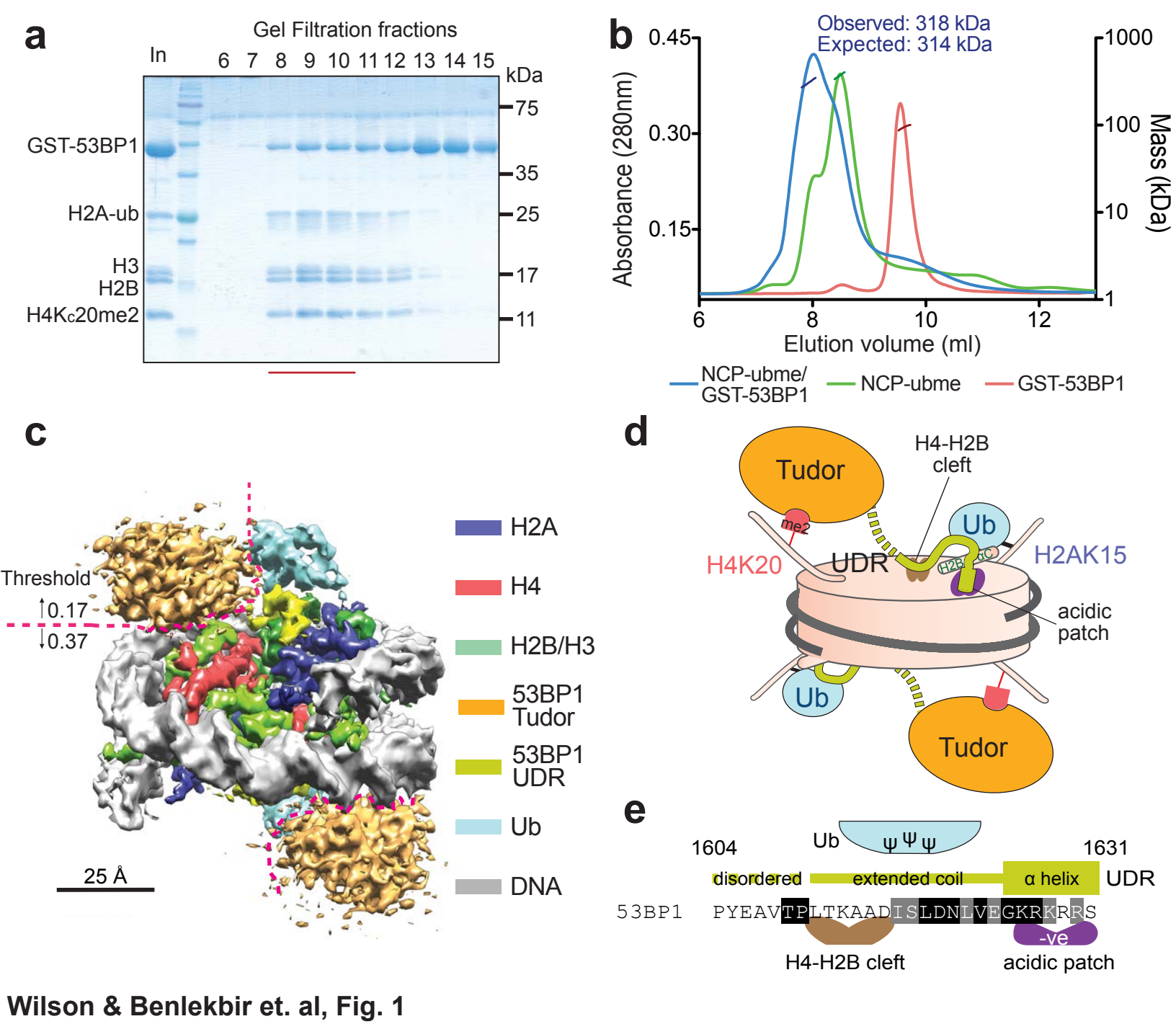

Wilson & Benlekbir et. al, Fig. 1

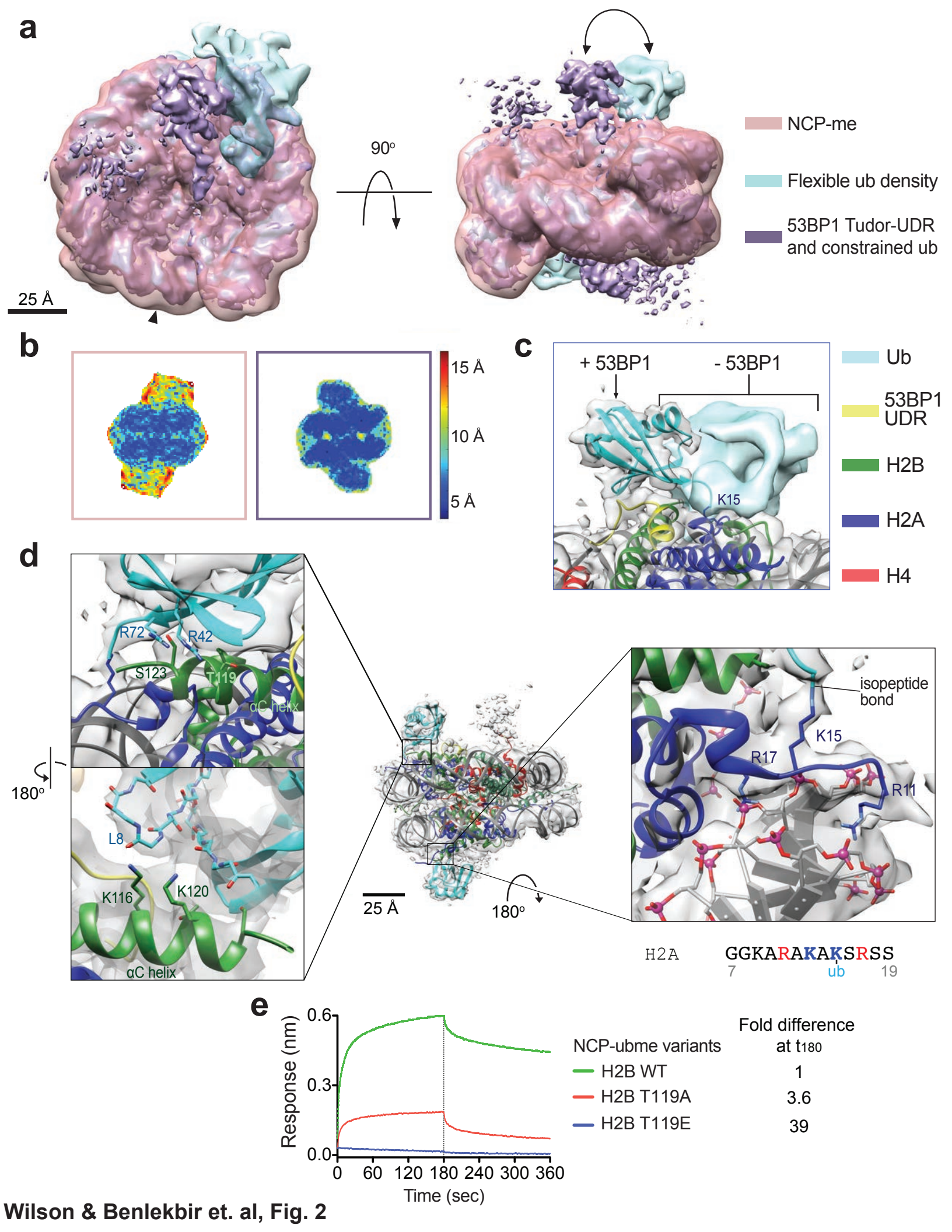

Wilson & Benlekbir et. al, Fig. 2

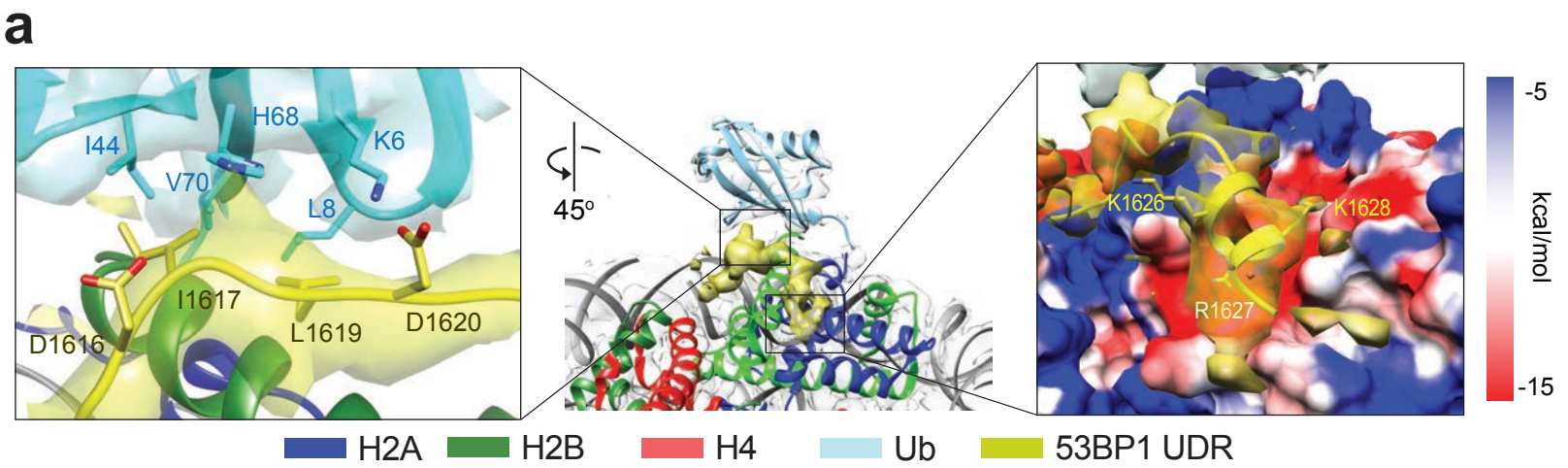

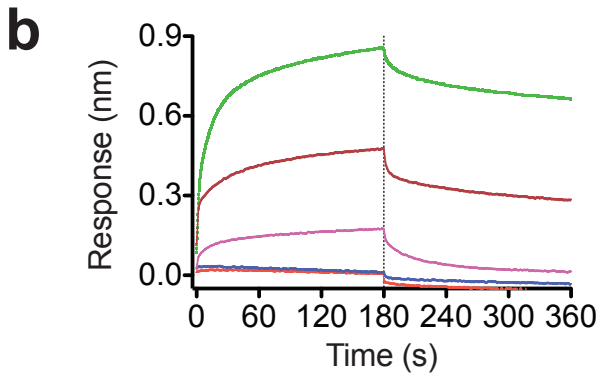

GST-53BP1 variants	Fold difference at t_{180}
WT	1
D1616A/1620A	2.0
D1616K/1620K	4.9
L1619A	75
I1617A	103

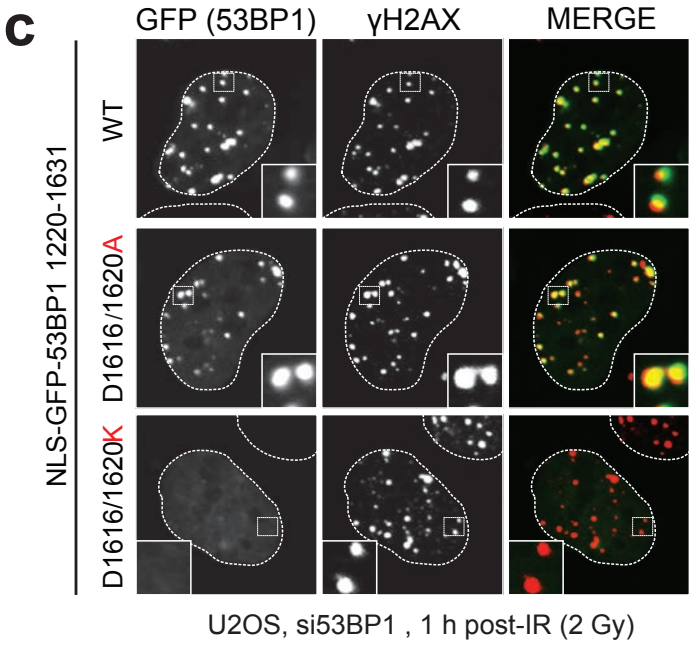

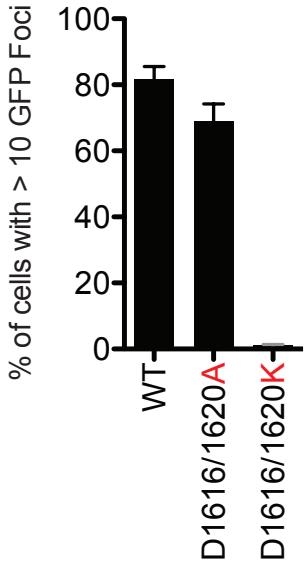

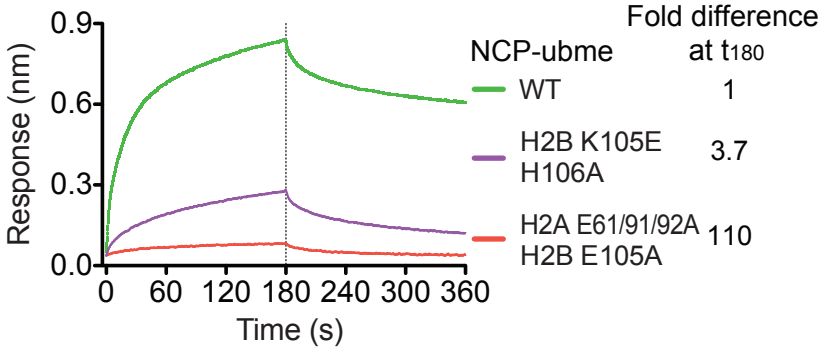

NCP-ubme	Fold difference at t_{180}
WT	1
H2B K105E H106A	3.7
H2A E61/91/92A H2B E105A	110

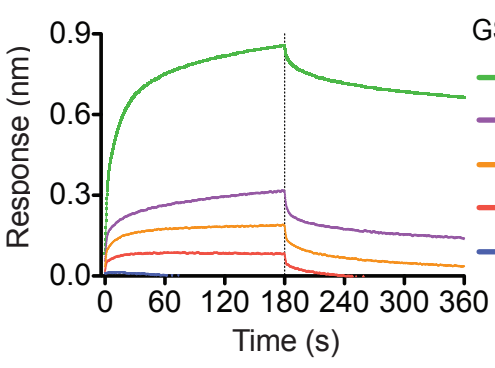

GST-53BP1	Fold difference at t_{180}
WT	1
K1628C	2.7
R1629A	4.5
K1626A	12
R1627A	NB

Wilson & Benlekbir et. al, Fig. 3

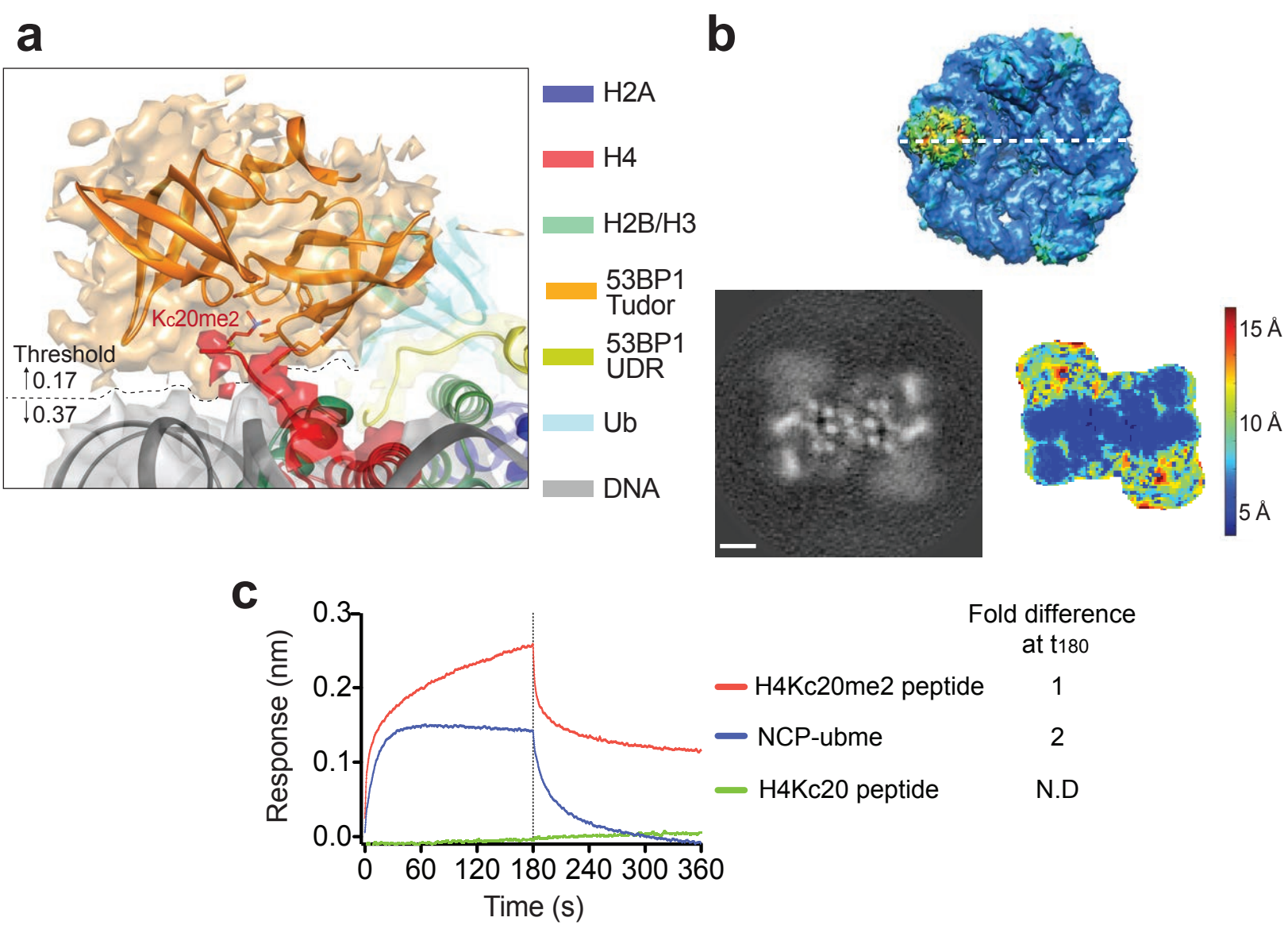

Wilson & Benlekbir et. al, Fig. 4

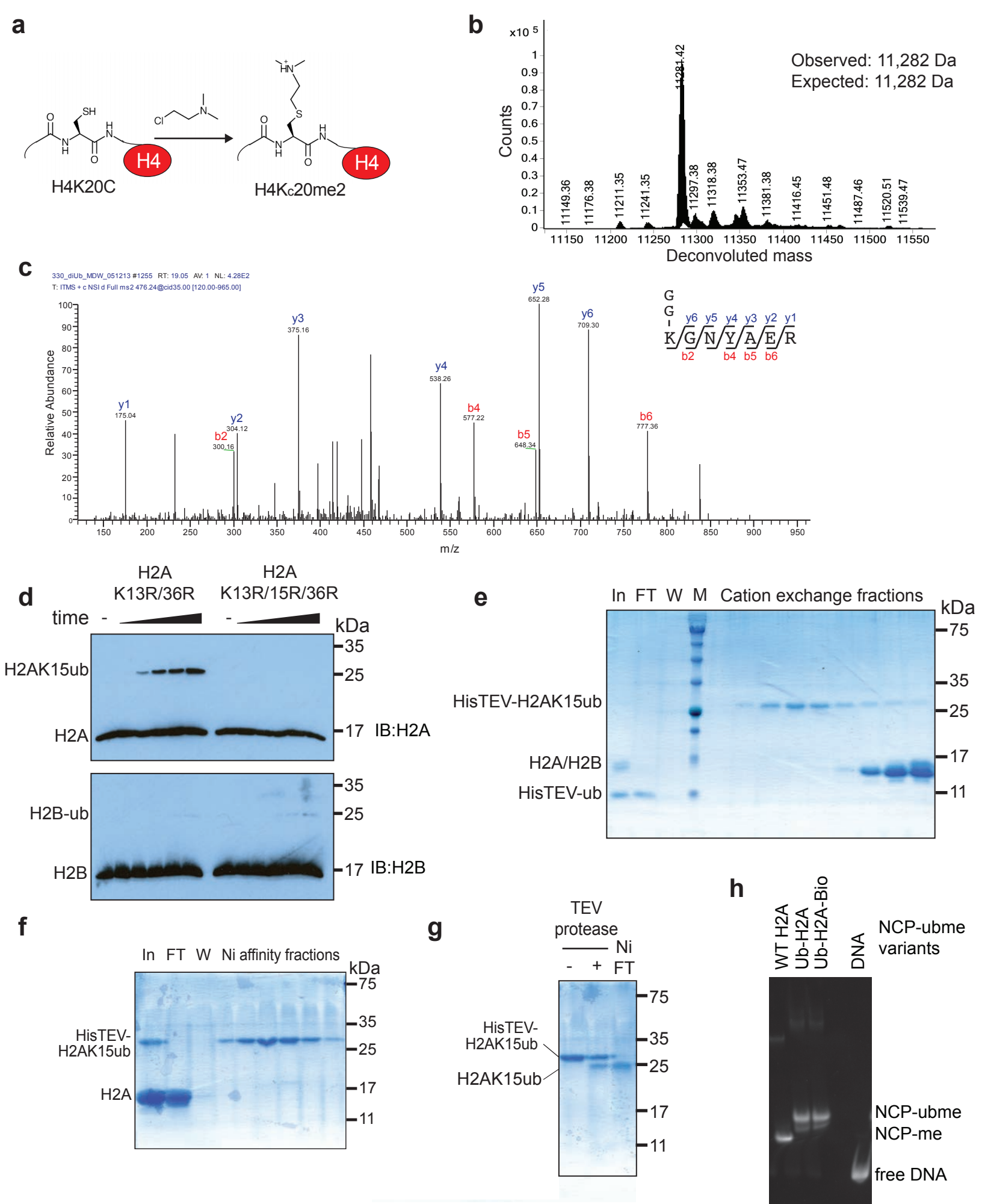

Wilson & Benlekbir et. al, Extended data Fig. 1

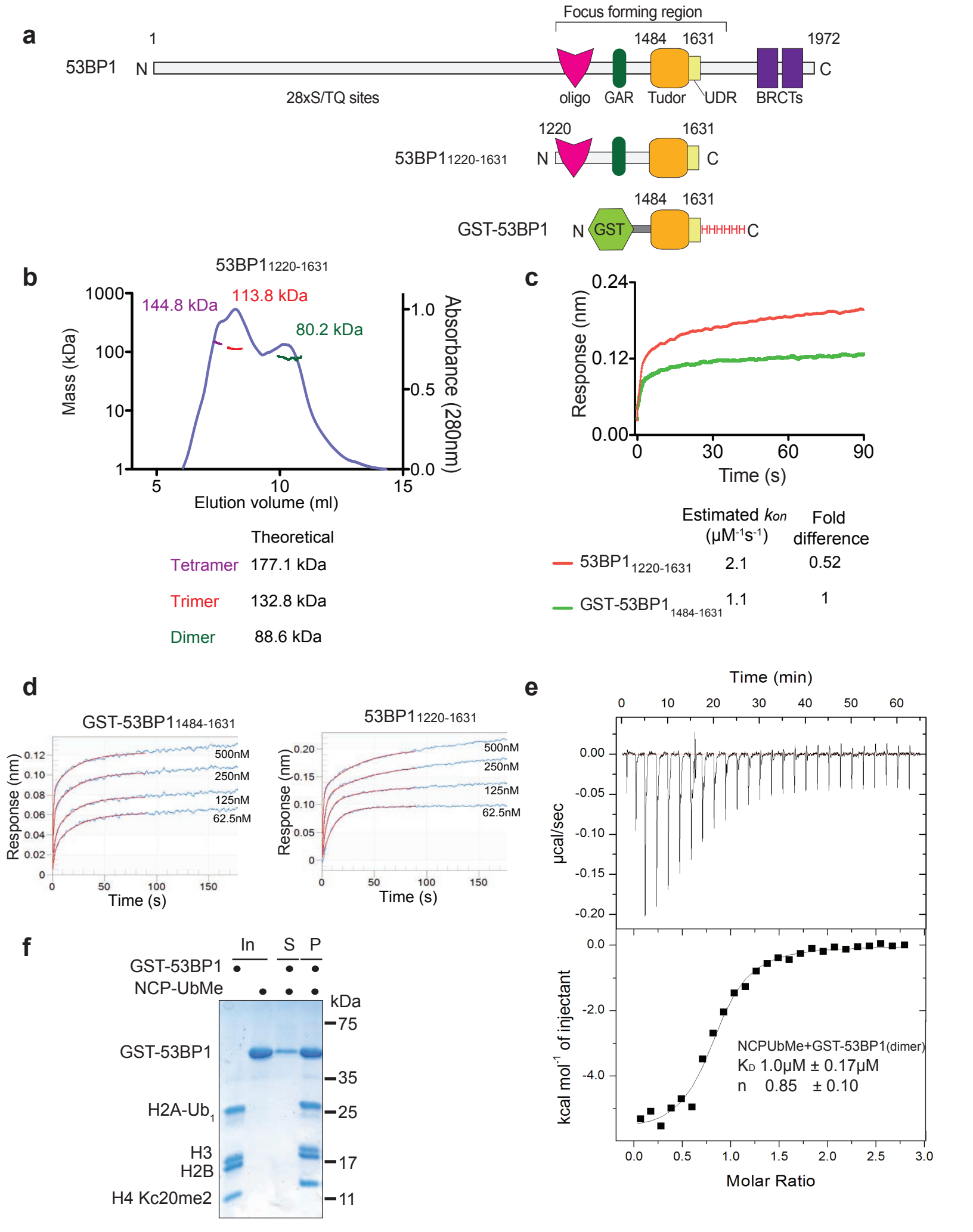

Wilson & Benlekbir et. al, Extended data Fig. 2

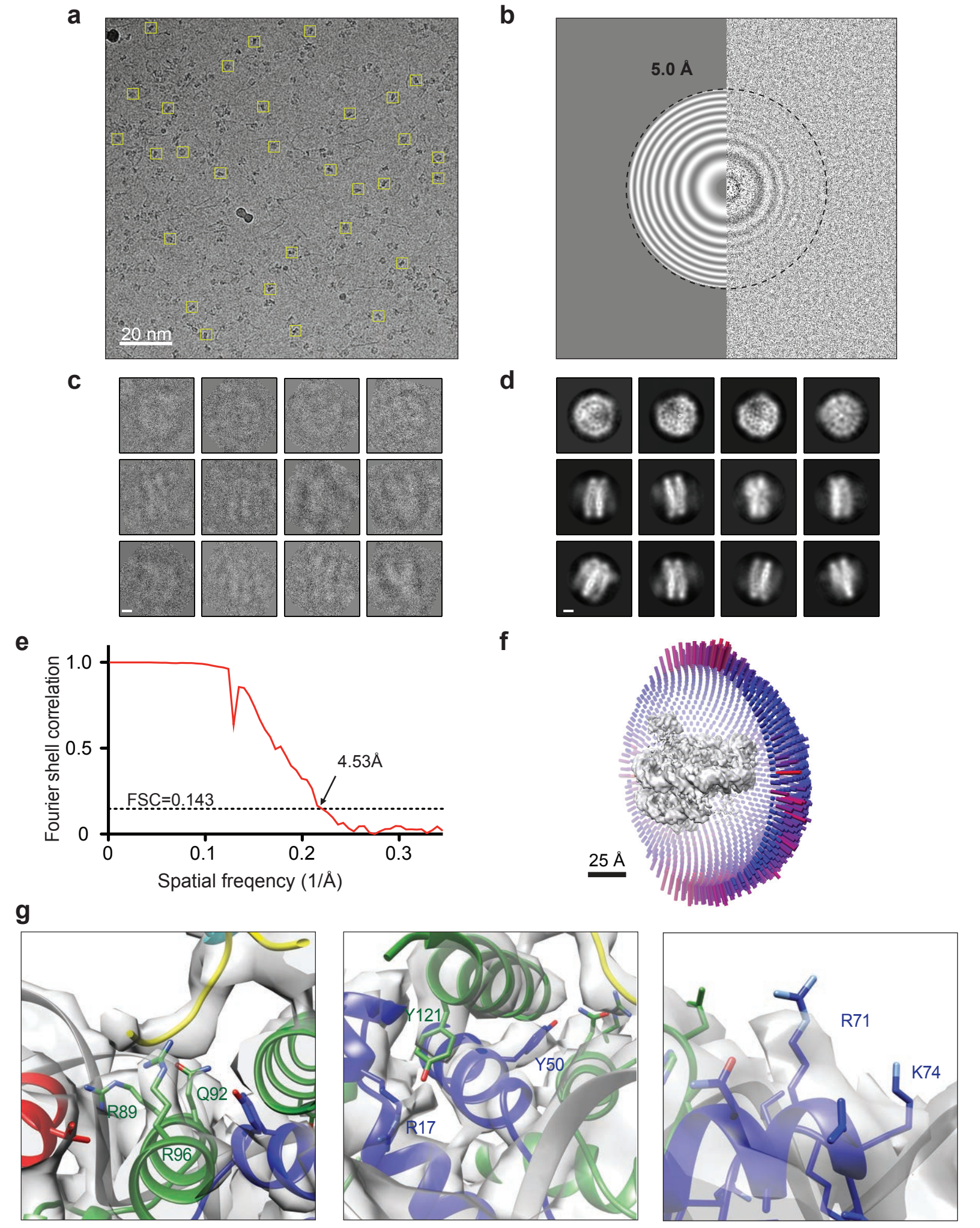

Wilson & Benlekbir et. al, Extended data Fig. 3

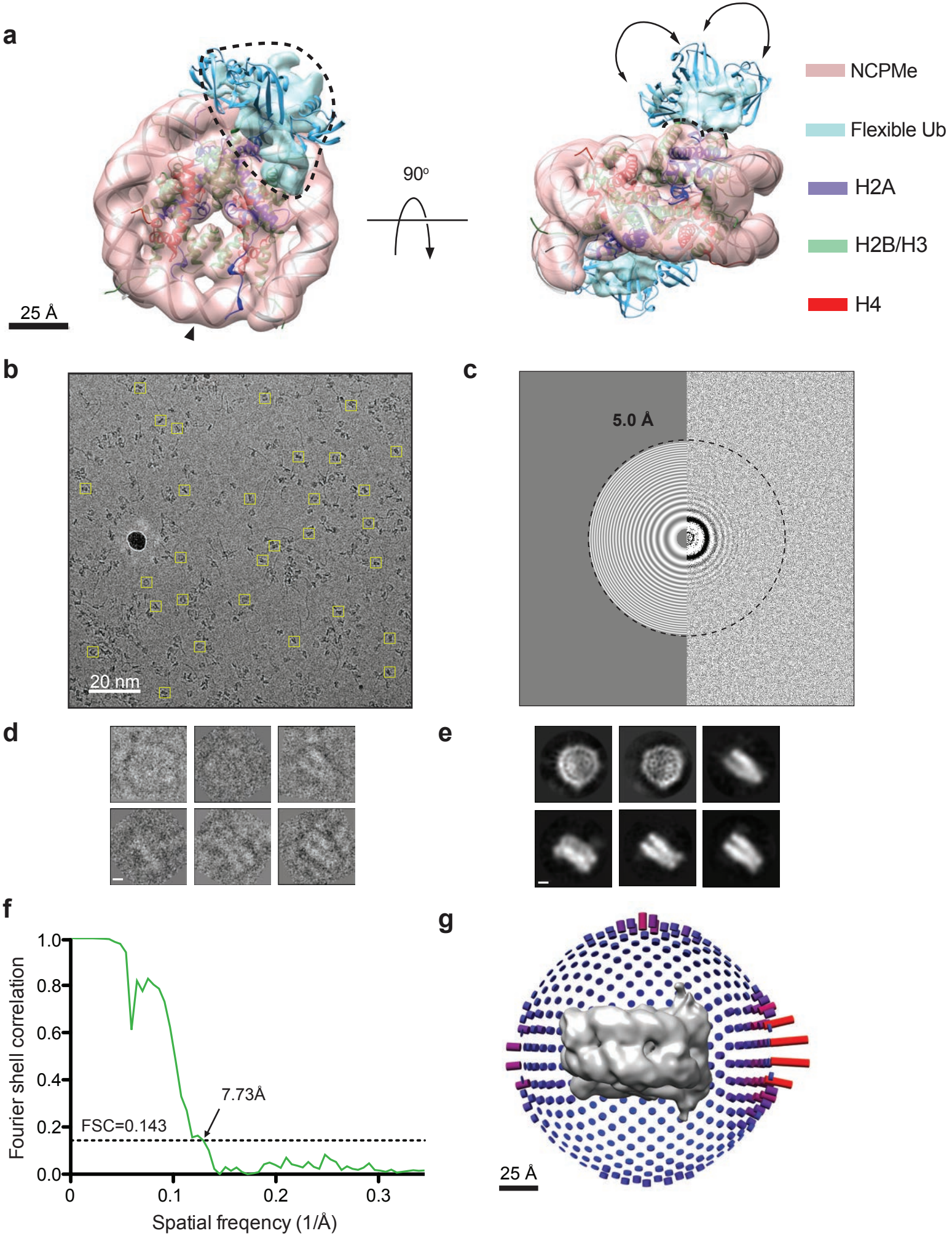

Wilson & Benlekbir et. al, Extended data Fig. 4

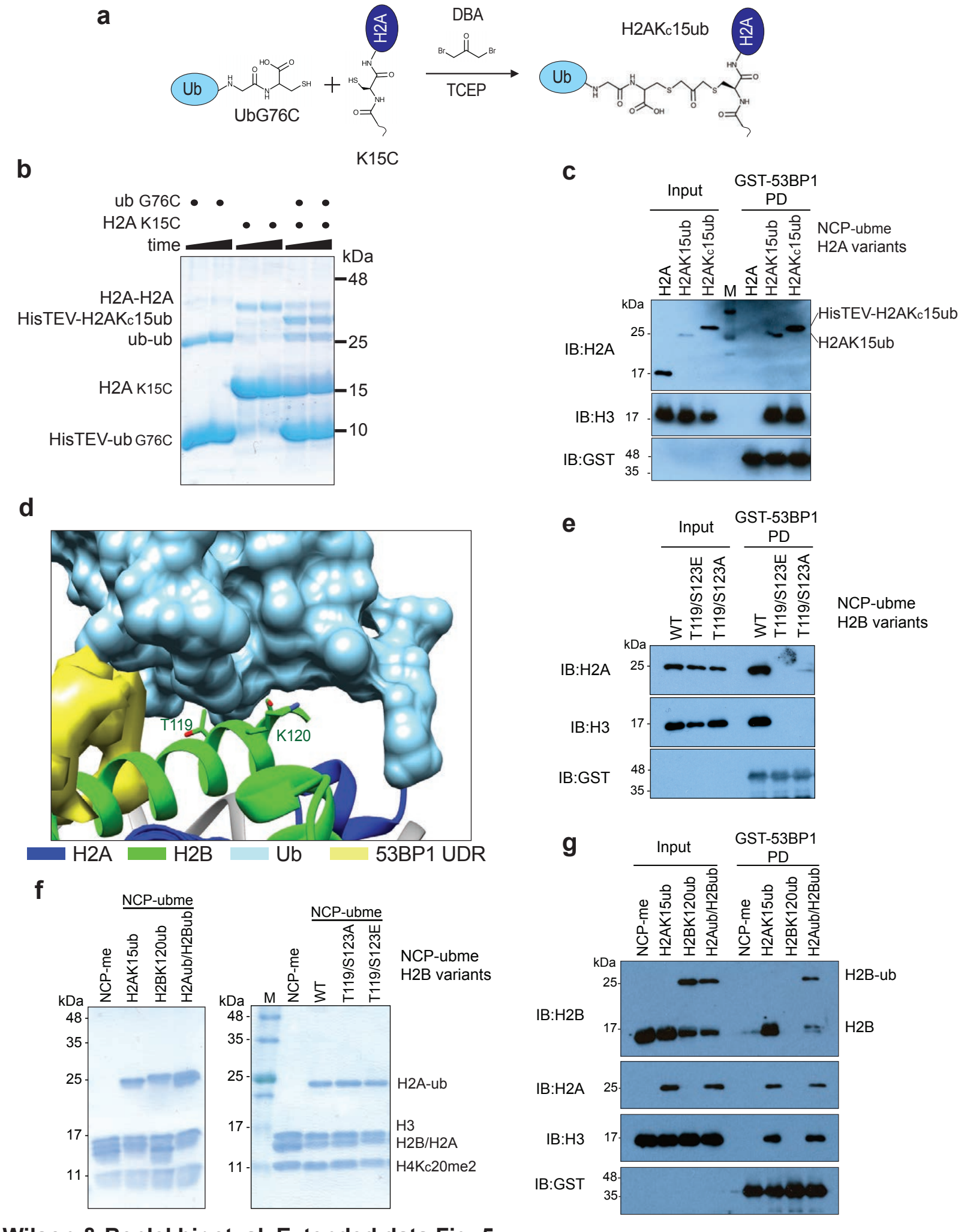

Wilson & Benlekbir et. al, Extended data Fig. 5

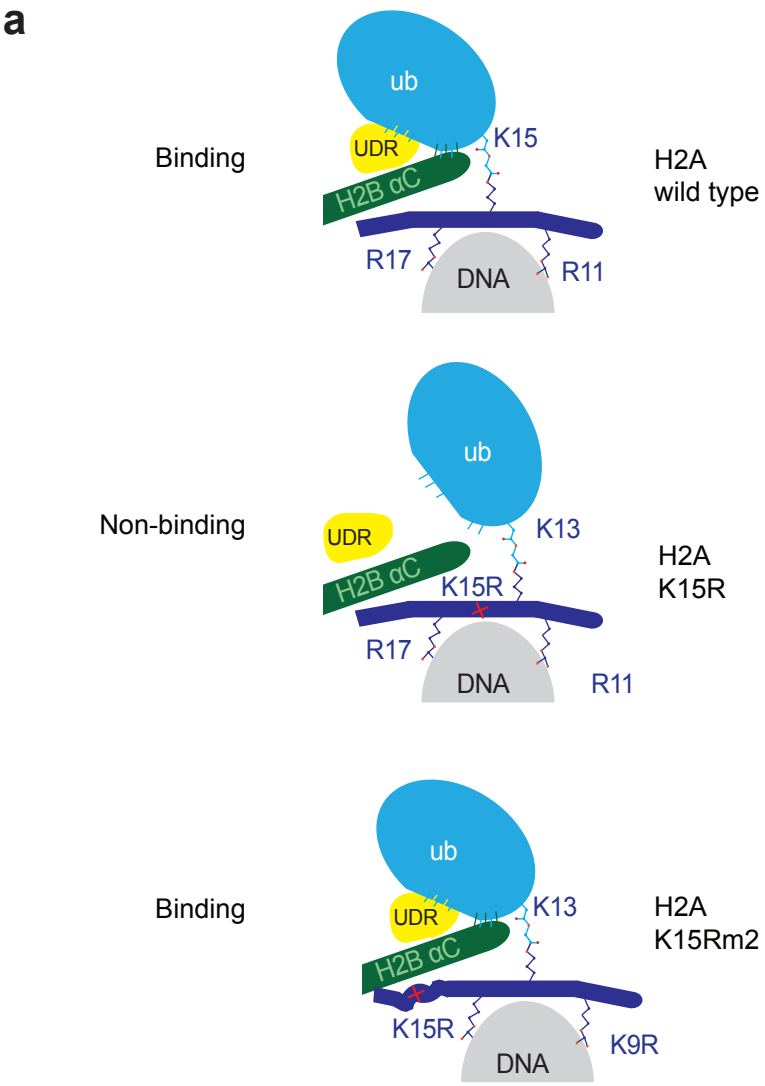

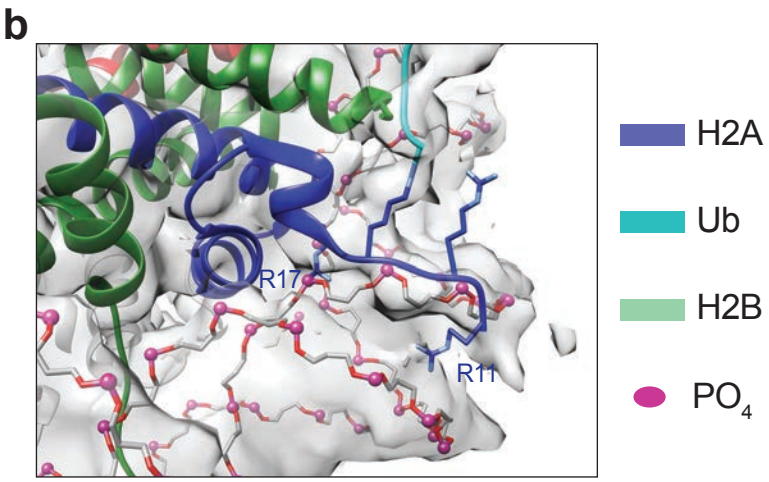

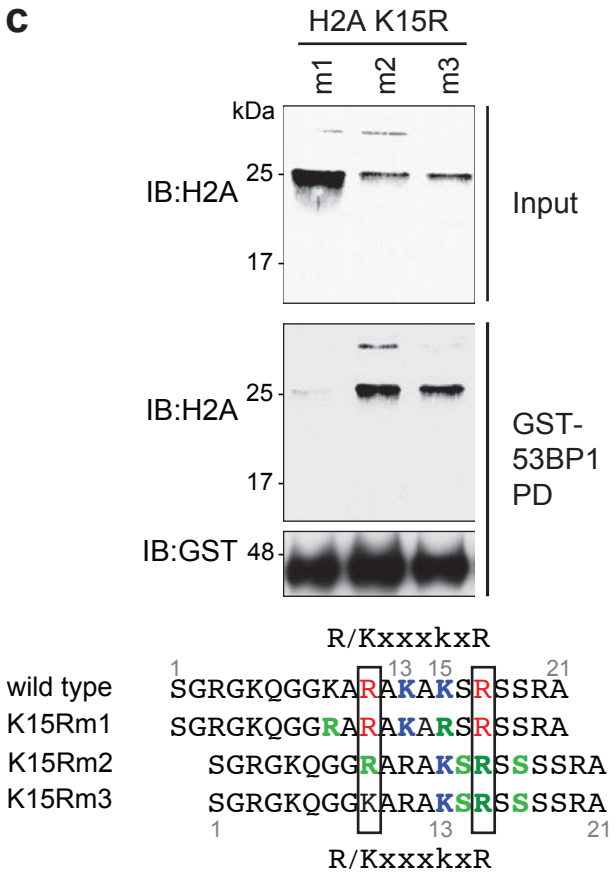

Wilson & Benlekbir et. al, Extended data Fig. 6

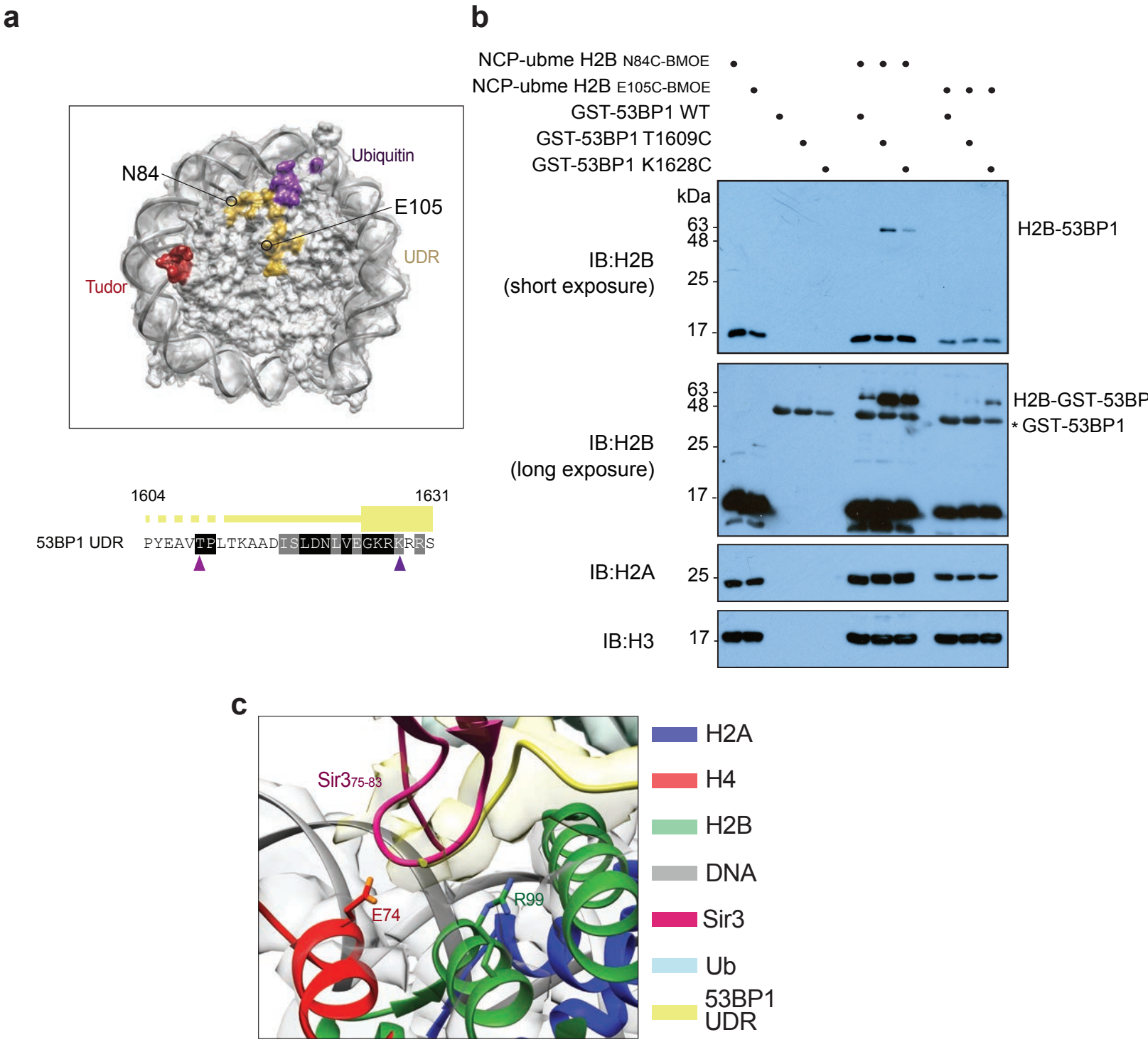

Wilson & Benlekbir et. al, Extended data Fig. 7

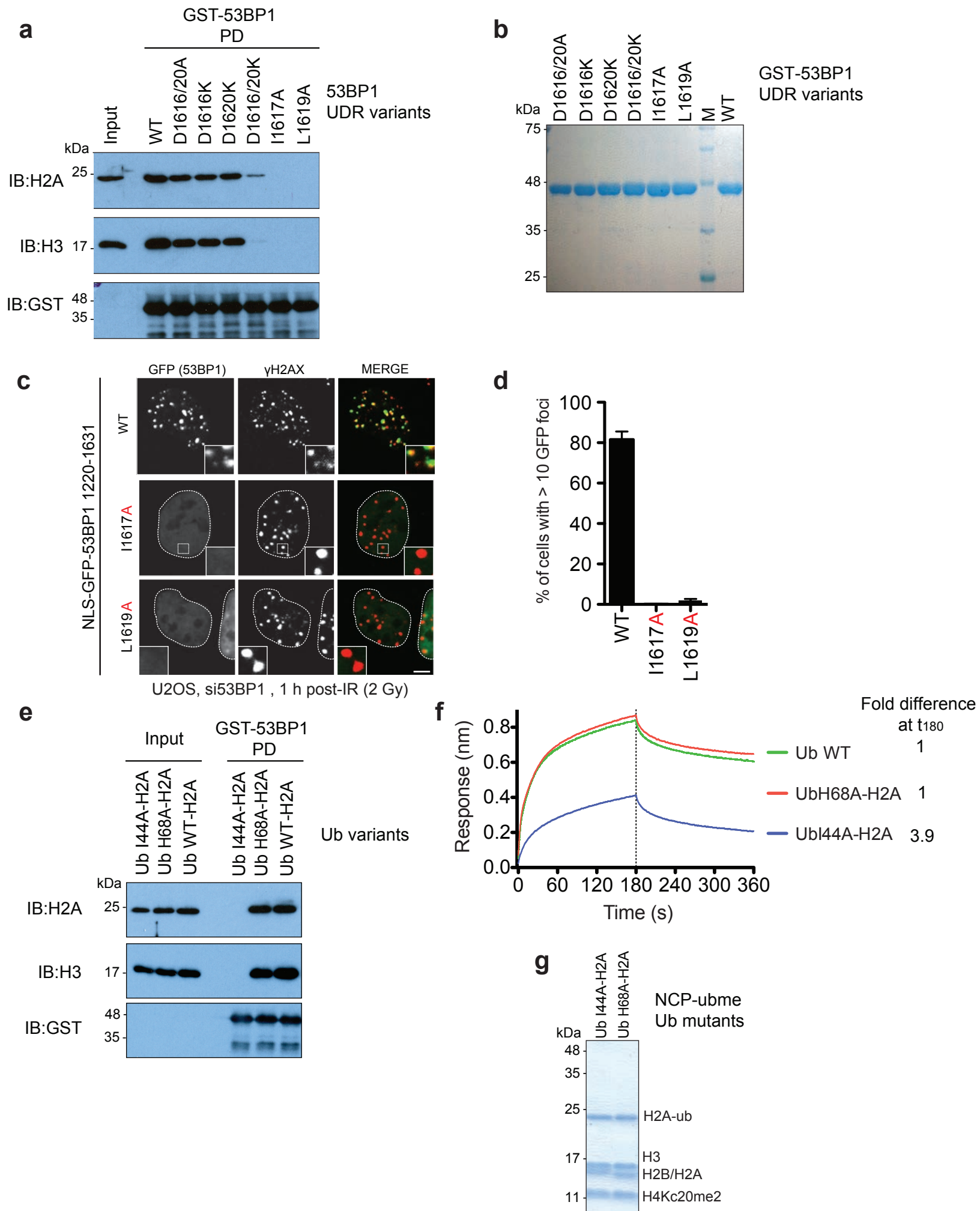

Wilson & Benlekbir et. al, Extended data Fig. 8

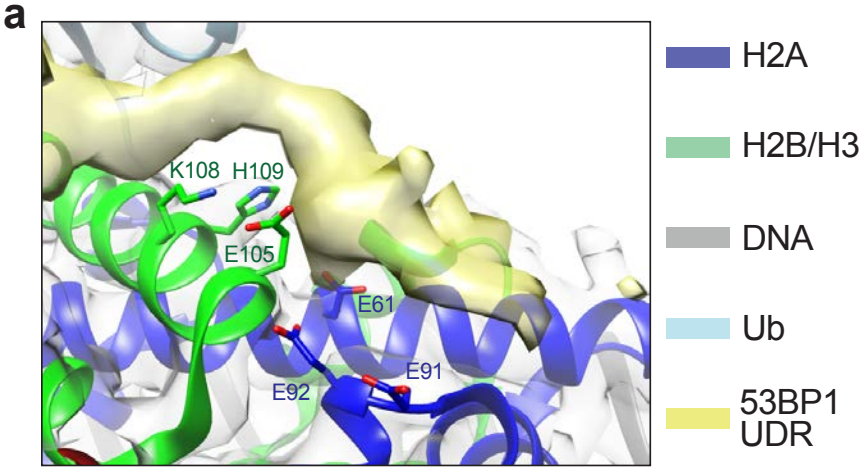

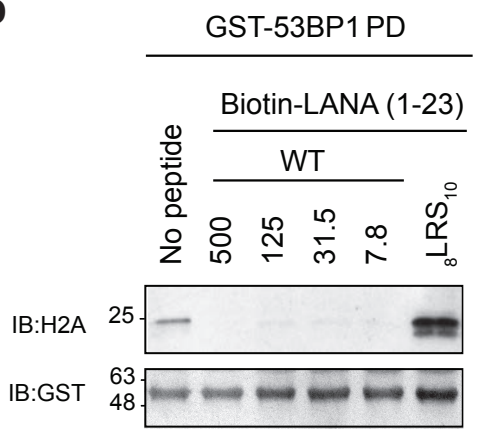

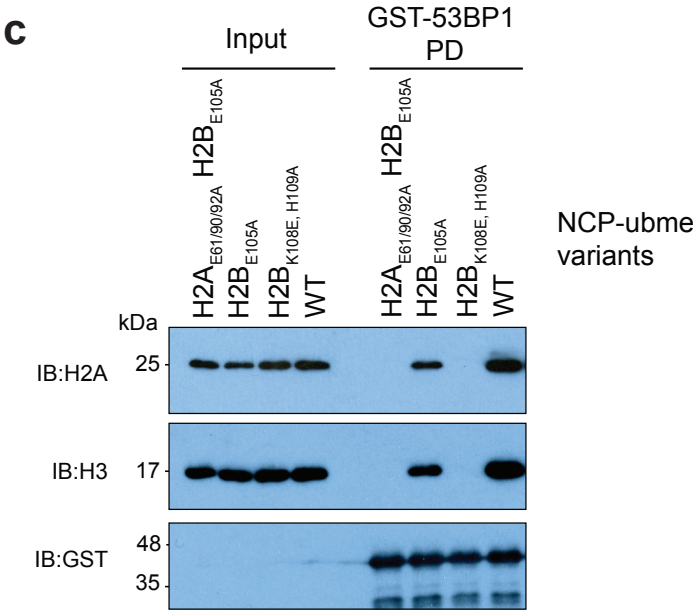

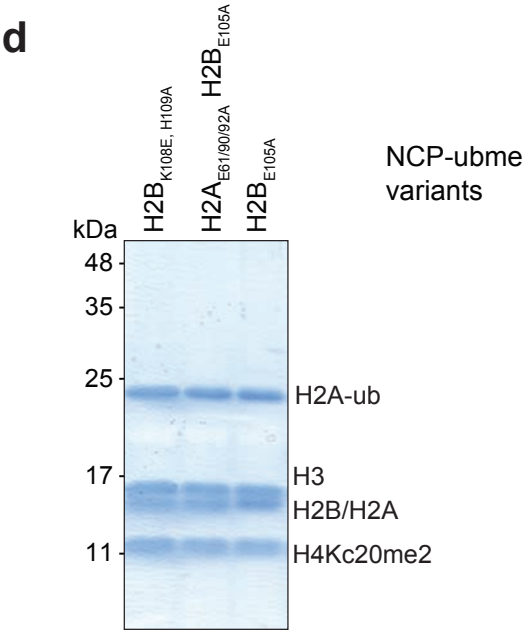

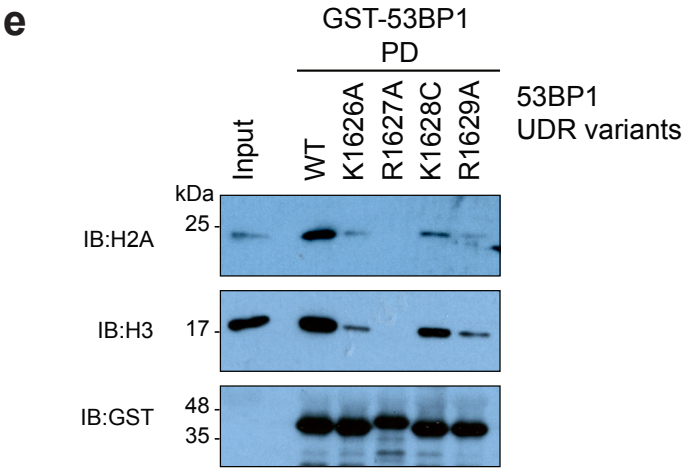

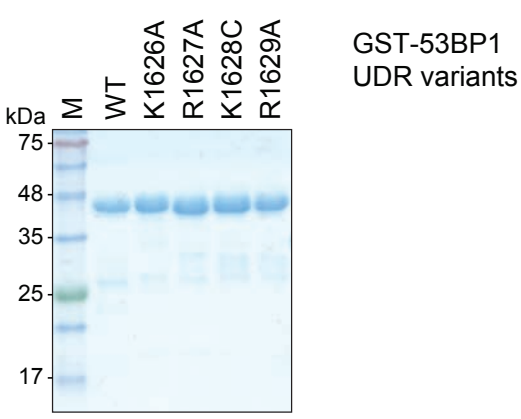

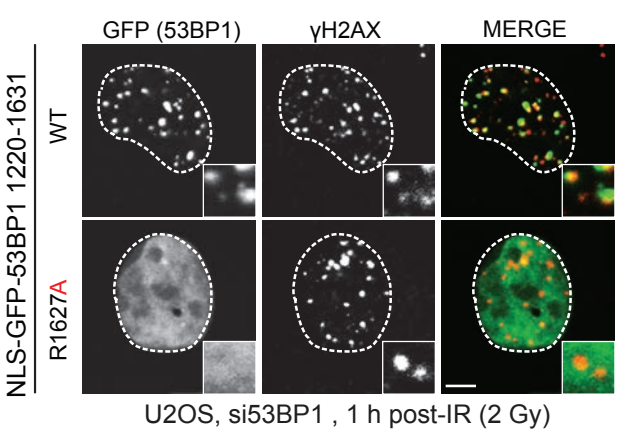

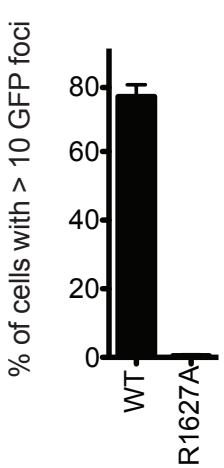

Wilson & Benlekbir et. al, Extended data Fig. 9

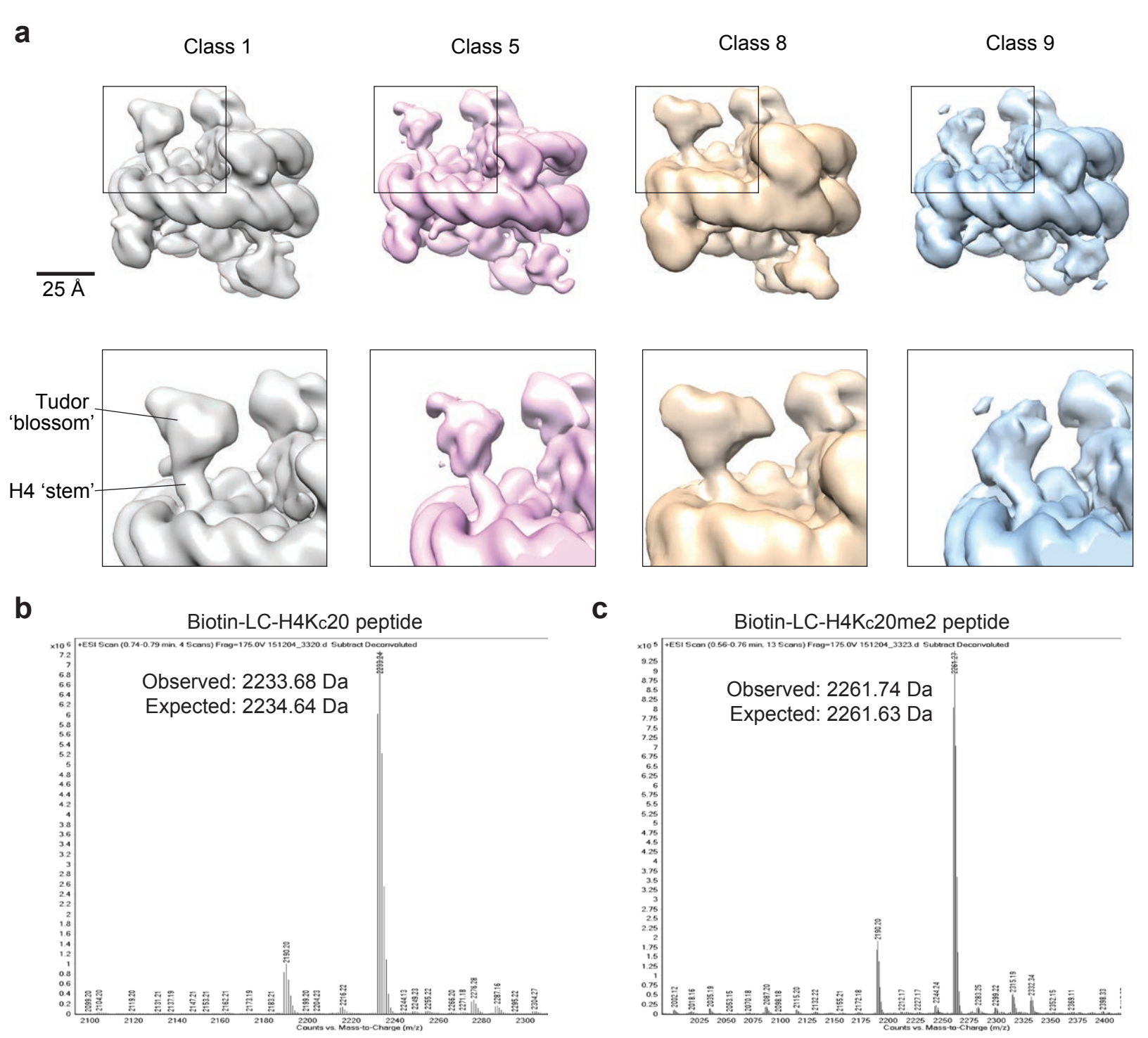

Wilson & Benlekbir et. al, Extended data Fig. 10